

REDEFINING MULTIDRUG RESISTANCE IN CANCER

by

ASHLEY ELIZABETH RAY

(Under the Direction of Eugene Douglass)

ABSTRACT

Multidrug resistance (MDR) is a primary barrier to successful cancer treatment with small molecule drugs. One mechanism of resistance is through transporters which pump drug out of cancer cells before they exert any therapeutic effect. The most studied transporter is P-glycoprotein (Pgp), a member of the ATP Binding Cassette (ABC) superfamily of drug pumps. Prior research has focused on determining whether drugs are substrates of Pgp. Pgp specificity for FDA approved drugs is currently unclear due to technical variability in assays that quantify enzyme kinetics using non-cellular experimental models. Other approaches for overcoming MDR yielded selective Pgp inhibitors to increase intracellular drug accumulation. However, these selective inhibitors failed clinically. A quantitative, multifaceted approach is needed to characterize the MDR phenotype in cancer and optimize drug selection. Studying Pgp in the context of MDR, we improved Pgp specificity scores by leveraging new Pgp expression (cell lines, tissues) and function (drug screening) datasets. We experimentally and computationally integrated functional dataset information to better understand Pgp specificity using an approach based on underlying Michaelis-Menten enzyme kinetics. We obtained consensus scores for Pgp specificity across ~150 FDA approved oncology drugs and validated them experimentally in a subset of 76 substrates selected to represent the spectrum of drugs for Pgp specificity. These

scores can be used to calibrate clinical diagnostics (Pgp expression), and our experimental platform can be used to quantify Pgp function in clinical samples. Overall, we have developed a parallel computational and experimental procedure to estimate Pgp selectivity in live cells. This procedure can be expanded to other drug transporters which contribute to MDR to further characterize this phenotype quantitatively.

INDEX WORDS: Multidrug resistance, MDR, P-glycoprotein, Pgp, Cancer, Specificity

REDEFINING MULTIDRUG RESISTANCE IN CANCER

by

ASHLEY ELIZABETH RAY

BS, Mercer University, 2017

A Dissertation Submitted to the Graduate Faculty of The University of Georgia in Partial
Fulfillment of the Requirements for the Degree

DOCTOR OF PHILOSOPHY

ATHENS, GEORGIA

2024

© 2024

Ashley Elizabeth Ray

All Rights Reserved

REDEFINING MULTIDRUG RESISTANCE IN CANCER

by

ASHLEY ELIZABETH RAY

Major Professor: Eugene Douglass
Committee: Arthur Edison
Kosuke Funato
Y. George Zheng

Electronic Version Approved:

Ron Walcott
Vice Provost for Graduate Education and Dean of the Graduate School
The University of Georgia
December 2024

DEDICATION

I dedicate this dissertation to my family: my parents, Douglas and Susie, twin brother, Jordan, and late grandfather, William R. Crawford Jr. I am grateful for their love and support throughout my life including my Ph.D. program. To my Dad and Grandfather, who supported my interests in pharmaceutical industry research and development through their own successful careers with Pfizer in pharmaceutical sales. To my Mom and Jordan, who shared the ups and downs of my graduate school experience through countless conversations.

ACKNOWLEDGEMENTS

I would like to thank—

My major professor, Dr. Eugene Douglass, for taking a chance on me as his first graduate student in the Douglass Lab.

The current and former members of the Douglass Lab.

The staff in the University of Georgia College of Pharmacy for their support and hard work, in particular: Deborah Martinez and Brad Brown.

My colleagues in the University of Georgia Office of Research for supporting my professional endeavors and including me as part of their team.

The University of Georgia Graduate School for offering professional and career development opportunities for graduate students.

The professional connections I have made through graduate school, for their support, advice and encouragement, to name a few: Dr. Marty Bink, Dr. Larry Hornak, Dr. Crystal Leach, Dr. Jennifer Walker, Dr. Andrew Crain and Dr. Ken Blank.

My family and life group at Beech Haven Church in Athens for encouraging me in the Bible through their words, prayers, humor and actions.

God, for growing my faith in graduate school, guiding me through life, reminding me that I am never alone, and He can use every circumstance for good.

TABLE OF CONTENTS

	Page
ACKNOWLEDGEMENTS	v
LIST OF TABLES	vii
LIST OF FIGURES	viii
CHAPTER	
1 MULTIDRUG RESISTANCE	1
Cancer Multidrug Resistance	1
MDR Transporters	3
Overcoming MDR	6
2 COMPUTATIONAL DATABASES	12
DrugBank	12
CTRP, GDSC and PRISM	19
CCLE	23
3 QUANTITATIVE METRICS	26
Multidrug Resistance Overview	26
Potential for Functional Scoring	38
Experimental Work to Quantify MDR	57
REFERENCES	66
APPENDICES	79
A PROTOCOLS	79

LIST OF TABLES

	Page
Table 1: Taxane DrugBank Data	13
Table 2: Anthracycline DrugBank Data	14
Table 3: Vinca Alkaloid DrugBank Data.....	15
Table 4: DrugBank Data Entries.....	16
Table 5: Drug Screening Databases.....	20
Table 6: Cancer Cell Line Database	24

LIST OF FIGURES

	Page
Figure 1: Drug Efflux Mechanism.....	2
Figure 2: Structure of Drug Transporters.....	5
Figure 3: Function of Drug Transporters.....	6
Figure 4: Patient Selection for Therapies.....	9
Figure 5: Mathematics of Drug Dose Response.....	27
Figure 6: Pgp Normal Expression in Tissues.....	28
Figure 7: Drug Dose Response in MDR.....	31
Figure 8: BRENDA Enzyme Kinetics Data.....	34
Figure 9: DrugBank MDR Genes and Drugs.....	37
Figure 10: Mathematically Modeling MDR.....	40
Figure 11: Correlation Analysis to Fill Gaps.....	42
Figure 12: Quantitative Rankings of Drugs.....	44
Figure 13: Quantitative Metrics for Substrate Specificity.....	45
Figure 14: Approaches for Substrate Specificity Metrics.....	50
Figure 15: Limitations of AUC in Drug Screening.....	52
Figure 16: Fluorescent Probes for Drug Screening.....	55
Figure 17: Experimental Pipeline for Assay Development.....	58
Figure 18: Drug Screen Measures Potency.....	59
Figure 19: Drug Screen Measures Efficacy.....	61

CHAPTER 1

MULTIDRUG RESISTANCE

Subsection 1: Cancer Multidrug Resistance (MDR)

MDR is the ability of cancer cells to withstand a variety of chemotherapeutic drugs that differ in structure and mechanism (1). This resistance is a significant cause of treatment failure in cancer therapy, especially in metastatic and recurrent cancers. MDR contributes to poor prognosis in many cancers, such as leukemia, breast cancer, and lung cancer. It involves multiple, adaptable cellular mechanisms which make it challenging to manage clinically.

In the 1960s, resistance was a known phenomenon in the context of individual oncology drugs but not its mechanisms (2-4). A 1968 study was conducted to assess Daunomycin in mouse leukemic cells through uptake and retention. This study sought to determine correlations between the drug response and drug administered *in-vitro* or *in-vivo*. Ultimately, researchers concluded that drug response was more correlated to loss of drug from previously loaded *in-vivo* cells than uptake. Additionally, Kessel *et. al.* stated, “the amount of drug initially accumulated *in-vivo* was not a predictive index of drug response”. This indicates the presence of some mechanism that alters the amount of drug available for therapeutic effect (5). Another study was performed in 1970 to determine cross-resistance to Vincristine and Daunomycin with Actinomycin D using parent and drug-resistant cell lines. The discovery of cross-resistance suggested a common mechanism of resistance to all three drugs. Researchers postulated that alterations in the cell membrane made it less permeable to drug entry (6).

In 1973, a study was undertaken to follow up results showing decreased uptake of

Daunomycin in resistant vs wildtype ascites tumor cells (7). Researchers already knew of cross-resistance between Daunomycin, other anthracyclines and vinca alkaloids. They co-administered Daunomycin with each of the cross-resistant drugs in the resistant lines. For most drugs, they increased Daunomycin uptake in the resistant lines which indicated competitive inhibition. Additional experiments were performed to study effects

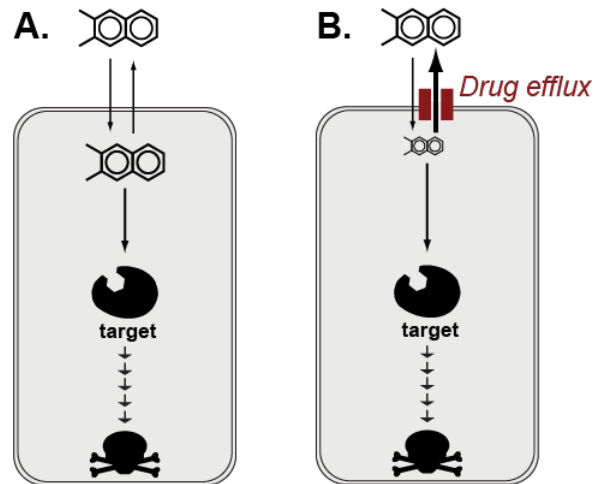


Figure 1. Drug Efflux Mechanism. (A) Normal cells accumulate drug which targets the cells and causes cell killing. (B) Efflux decreases drug accumulation in multidrug resistant cells.

of metabolism on Daunomycin uptake and intracellular localization. Taken together, Danø provided “higher efficiency of the active...extrusion, a decreased influx (in presence of active extrusion), or both” as explanations for Daunomycin resistance. Thus, resistance was linked to decreased drug accumulation in cells, suggesting the presence of a drug efflux mechanism as shown in Figure 1 (7).

In 1974, researchers used Colchicine-resistant Chinese Hamster cell clones to test alterations to Colchicine binding to its intracellular target and prior theories on membrane permeability (8). Interestingly, they did not find any changes to Colchicine-intracellular target binding between wildtype and resistant lines. Their research showed reductions in Colchicine uptake in the resistant lines which supports a permeability resistance mechanism. Additional findings demonstrated a positive correlation between Colchicine resistance and cross-resistance. It also elucidated a negative correlation between Colchicine resistance and uptake. This work set

the stage for more *in-vitro* work using cell lines with variations of the drug-resistant phenotype (8).

Prior studies (5-8) pointed conclusively to membrane permeability as the source of drug resistance. Thus, a 1974 study expanded on this theory by studying the exact mechanism of Colchicine uptake in Chinese Hamster Ovary cells. Experiments supported a diffusion mediated mechanism including nonsaturation kinetics of Colchicine uptake and no change in uptake with inclusion of structural analogs. Additionally, the use of membrane detergents stimulated Colchicine uptake along with co-administration of other drugs. This work introduced kinetics and energy dependence on ATP into discussions on drug resistance. Lastly, Carlsen *et. al.* mentioned the observation of “a glycoprotein of approximately 170,000 daltons...exposed at the surface of colchicine resistant mutants and is absent or in greatly decreased amounts in the wild-type cells”. This first posited glycoproteins as the membrane proteins responsible for reducing intracellular drug accumulation (9).

Subsection 2: MDR Transporters

In 1976, researchers again identified a cell surface glycoprotein measuring 170,000 Daltons in resistant clones of Chinese Hamster Ovary cells (10). From cell surface labelling studies, this glycoprotein was largely absent from the parent line but present in the resistant lines. Researchers discovered a strong, positive correlation between the expression of this glycoprotein and drug resistance. Since the presence of this glycoprotein altered membrane permeability, they named it the Permeability or P-glycoprotein (Pgp). To determine Pgp amounts in other cells, an Actinomycin D and cross-resistant Syrian hamster line, SV40, and its parent line were examined. Compared to its parent line, the SV40 cells had increased amounts of membrane glycoproteins. This demonstrated the presence of Pgp in MDR cell lines. Researchers theorized that Pgp and

other glycoproteins were reducing plasma membrane permeability to drugs. They also noted that these glycoproteins were influenced by ATP levels (10).

To follow up previous studies, researchers made their first attempt at purifying Pgp from Chinese Hamster Ovary cells in 1979 (11). Plasma membrane vesicles were isolated through cell disruption and a series of centrifugation and washing steps. Membrane proteins were extracted through centrifugation, dialysis, detergents and lectin-agarose chromatography. Although the purification process was not 100% pure, this was a starting point for isolating Pgp for additional study. To that extent, this work presented the purification of Pgp and suggested future avenues for reconstituting it using *in-vitro* systems (11).

These studies are among others in the 1970s-1980s (12-15) that demonstrated Pgp could actively transport drugs out of cells, leading to reduced cytotoxicity and resistance to multiple drugs. In 1986, researchers used KB cells, a subline of HeLa cervical adenocarcinoma cells, to study genetic changes associated with MDR. Specifically, they noticed amplification of DNA sequences on the MDR gene locus, *MDR1*. Further examination demonstrated a 4.5 kilobase increased expression of *MDR1* messenger RNA (mRNA) followed by amplification of *MDR1* DNA. This research established Pgp as the first ATP Binding Cassette (ABC) transporter associated with MDR with characterization of its gene and protein (16).

Pgp is a 170 kDa (9-10) membrane protein with two nucleotide binding domains (NBDs) and two transmembrane domains (TMDs) that utilize ATP hydrolysis to efflux substrates across the cell membrane. Pgp was shown to export a wide range of drugs, including chemotherapeutics like Doxorubicin, Vincristine and Paclitaxel, contributing to MDR in various cancers. Other transporters were soon discovered after Pgp such as Multidrug Resistance Protein 1 (MRP1) encoded by *ABCC1*. MRP1 was identified in the 1990s (17) as another key player in MDR. It

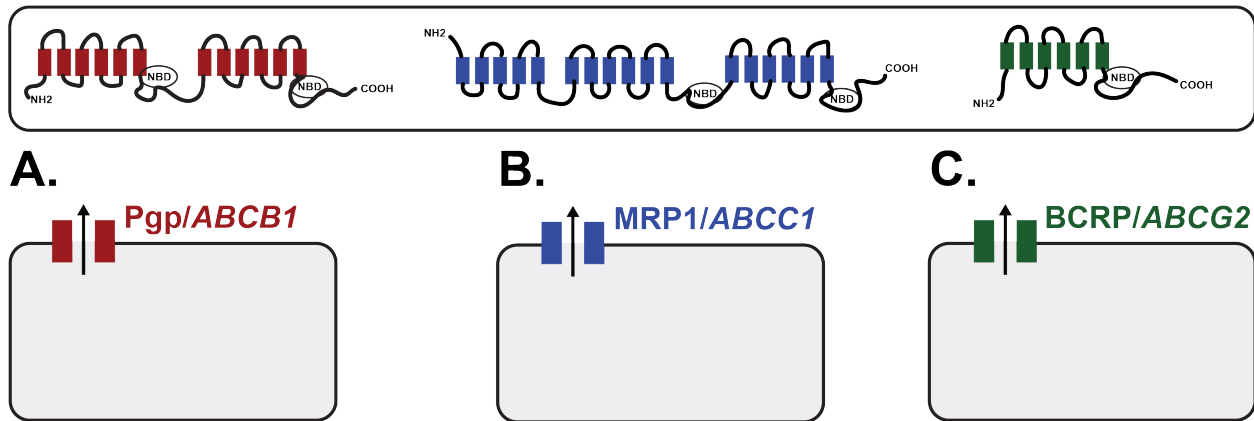


Figure 2. Structure of Drug Transporters. (A) Pgp has 12 transmembrane (TM) alpha-helices separated into 2 homologous halves with 2 nuclear binding domains (NBDs). (B) MRP1 has 17 TM alpha-helices separated into 3 TM domain sections of 5 and 6 TM alpha-helices with 2 NBDs. (C) BCRP has 6 TM alpha-helices and 1 NBD.

mediates resistance through the export of glutathione, glucuronide and sulfate conjugates. Unlike Pgp, MRP1 transports organic anions and conjugates, providing a different spectrum of resistance and indicating the diversity of the ABC transporter family (18). Another ABC transporter is Breast Cancer Resistance Protein (BCRP) encoded by *ABCG2* and discovered in the late 1990s by a few independent research groups (19-21). BCRP plays a role in resistance to drugs such as Mitoxantrone, Topotecan and Irinotecan. Unlike Pgp and MRP1, BCRP has just one NBD and one TMD. Its expression in tissues such as the placenta, liver and intestines indicate its role in both drug resistance and normal physiology (22). Figure 2 displays the structural differences between Pgp, MRP1 and BCRP in their TMDs and NBDs (23-29).

Although *ABCB1*, *ABCC1* and *ABCG2* are best known within the context of MDR, ABC transporters comprise seven subfamilies (ABCA to ABCG) which use ATP hydrolysis to transport various endogenous and exogenous substrates across cellular membranes. Beyond MDR, ABC transporters are involved in lipid transport, antigen presentation and the protection

of tissues such as the blood-brain barrier from toxins (30). As a transporter, Pgp functions primarily by exporting hydrophobic drugs and exhibits broad substrate specificity due to its large binding pocket. MRP1 specializes in the efflux of glutathione and glucuronide conjugates which contributes to resistance against drugs like Methotrexate and anthracyclines. BCRP is known for its ability to protect tissues from xenobiotics and plays a role in placental drug transport and intestinal absorption (31). Figure 3 demonstrates the functional differences between Pgp, MRP1 and BCRP with endogenous and exogenous substrates (32-40).

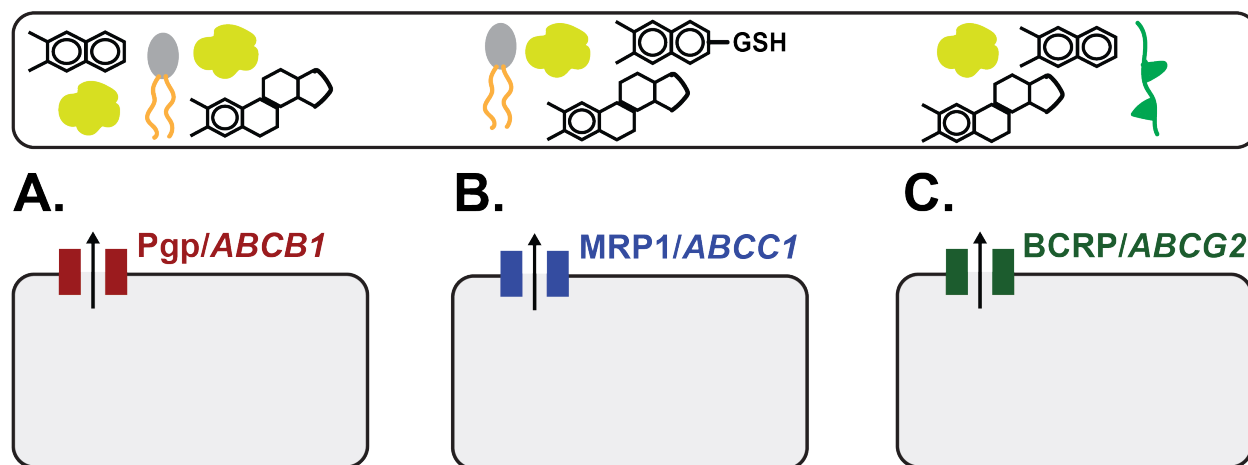


Figure 3. Function of Drug Transporters. Pgp, MRP1 and BCRP efflux various oncology and non-oncology drugs. (A) Pgp effluxes bile acids, bilirubin, steroids, and lipids. (B) MRP1 effluxes sulfate, glutathione and glucuronide conjugates, bilirubin, lipids, and steroids. (C) BCRP effluxes uric acid, flavonoids, bile, and steroids.

Subsection 3: Overcoming MDR

With the involvement of transporters in MDR, research moved toward development of Pgp inhibitors to reverse resistance. Drugs that act as Pgp inhibitors typically work through competitive or noncompetitive inhibition. Competitive inhibitors work by directly competing with drug for binding sites within Pgp. Noncompetitive inhibitors work by binding to ATP-

binding sites on the NBDs, so ATP cannot be hydrolyzed. Other noncompetitive inhibitors work by binding to allosteric sites changing Pgp's conformation (41-42).

To determine whether drugs acted as Pgp inhibitors, various assays have been employed over the years to test the inhibitory effects on Pgp function. These assays examined any changes in ATPase activity, efflux, intracellular accumulation and transport. For the assays, different techniques were used including photoaffinity labeling, monolayers, Pgp-specific antibodies and fluorescent probes among others (43).

Early inhibitors were drugs tested as Pgp inhibitors but faced challenges due to their lack of specificity and high toxicity. First generation inhibitors typically demonstrated some level of Pgp modulation whether as a competitive substrate or inhibitor. These first-generation inhibitors covered several classes including cardiac drugs, immunosuppressants, antibiotics, antifungals, antimalarials, antiprotozoals, antivirals, central nervous system depressants, anesthetics, antihistamines, oncology drugs and anti-inflammatory drugs. Some of the well-known first generation Pgp inhibitors are Verapamil, Nifedipine and Cyclosporine A. Second generation inhibitors were mainly derivatives of first-generation inhibitors such as stereoisomers. These derivatives include Dexverapamil, from Verapamil, and Valspodar, from Cyclosporine A (43-48).

Next generation inhibitors were more specific and showed initial promise in preclinical studies. But they largely failed in clinical trials due to adverse side effects or limited efficacy. Third generation inhibitors were designed for Pgp inhibition to maximize specificity over first- and second-generation inhibitors. The prevailing thought was co-administering a Pgp inhibitor with a small molecule drug would reverse MDR. These third-generation inhibitors include Zosuquidar, Elacridar, Tariquidar, ONT-093 and PGP-4008. Although more potent than previous

inhibitors, they did not yield any measurable clinical improvement in Phase I trials. Around 2010, the field pivoted away from development of Pgp inhibitors due to their failure in clinical trials (43,49-54).

Alternative approaches for overcoming MDR involved developing noncompetitive inhibitors and using combinatorial strategies. Combination treatments usually included immune checkpoint inhibitors. Unfortunately, competitive inhibitors directly compete with drug for Pgp binding and efflux which led to side effects. They can interfere with Pgp's normal physiological function or cause toxicity from intracellular overaccumulation of drug or endogenous substrate. Noncompetitive inhibitors modulate Pgp activity by interfering with ATP hydrolysis but not directly with drug binding (42,55).

In more recent years, research has focused on immune checkpoints and the interaction of immune cells with Pgp. Specifically, Pgp is differentially expressed in macrophages in tumors which can have different activities depending on phenotype. M1 macrophages inhibit cell proliferation and damage tissue whereas M2 macrophages stimulate cell proliferation and repair tissue (56). This opposing dichotomy has been studied in the context of drug transporter expression and Pgp. Interestingly, Pgp expression is upregulated in M2 and downregulated in M1 macrophages which contributes to cancer resistance. Thus, more research has centered on use of immune checkpoint monoclonal antibodies to target cytotoxic T-lymphocyte antigen 4 (CTLA-4), programmed cell-death protein 1 (PD-1) and PD-1 ligand 1 protein (PD-L1) in MDR. These monoclonal antibodies are not susceptible to efflux and can resensitize the antitumor response of cells (57).

The challenges in targeting ABC transporters stem from their complex role in physiology. They are essential for normal cellular functions and inhibiting them can lead to off-

target effects and toxicity. ABC transporters move endogenous substrates such as lipids, steroids and bile in addition to exogenous compounds out of cells.

Physiologically, they are involved in pharmacokinetics roles including absorption (intestines, colon), distribution, metabolism (liver) and excretion (kidneys) of drugs from the body. They have additional functionality in barrier tissues such as the brain, lungs and testes (58-59).

In these tissues, ABC transporters prevent toxic accumulation and maintain exchange of substrates between the tissues and bloodstream.

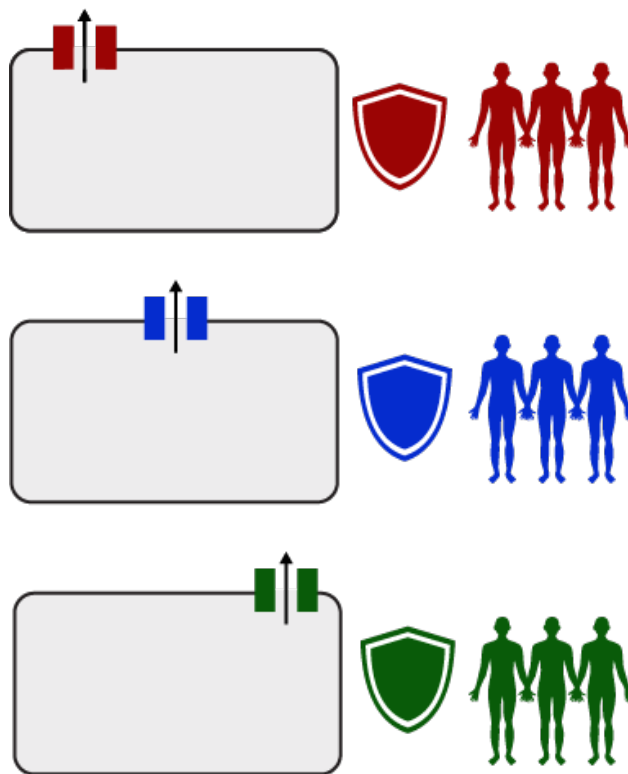


Figure 4. Patient Selection for Therapies. Different patients express different MDR genes in their cancer cells. ABC transporters can be used as biomarkers for optimizing drug selection in the clinic.

Thus, identifying reliable biomarkers for patient selection is crucial for the successful application of transporter targeted therapies (Figure 4). *ABC* genes in MDR are differentially expressed in patients depending on the cancer and tissues involved. Patient tumors can express combinations of MDR genes which can be up or downregulated from normal expression. Since transporters efflux different substrates, these drug pumps can be used as biomarkers to select the right therapy. For therapies that target transporters such as inhibitors and drugs which are known substrates, surveilling for biomarkers is critical. For instance, tumors high in Pgp only would be ideal candidates for a combination approach using a selective Pgp inhibitor and drug (60-61).

In the future, there must be an emphasis on understanding the tumor microenvironment, exploring immune cell interactions and developing targeted delivery systems. MDR is a complex phenomenon with multiple pathways that contribute to protective measures taken by cancer cells to ensure their survival. Further research into the tumor microenvironment encompasses studying tumor cell types, cell-cell communications, immune system involvement, metastasis etc. The immune system is complex as is its interactions with cancer cells and ways in which it promotes or suppresses the antitumor response. Targeted delivery systems include nanoparticles with drug, microRNA (miRNA) or other cargo which can be directed to specific tissues. All these approaches are currently being studied as options to treat cancer (62-64).

Other researchers are investigating genetic and epigenetic factors influencing transporter expression to identify new therapeutic targets (65). This research has moved toward studying regulation of MDR genes through small interfering RNA (siRNA) and miRNA including delivery of these RNAs through nanoparticles. Other epigenetic changes in cancer have been examined like alterations in transcription factors, DNA methylation, chromatin and regulation through bulk and single cell RNA sequencing. Specifically, research has focused on histone modifications which have been closely linked to cancer development and progression. These covalent histone modifications are accomplished through processes such as acetylation, methylation, phosphorylation and ubiquitination (66-67).

Over the past five decades, substantial progress has been made in understanding MDR transporters and their roles in drug resistance. Research expanded to ‘omics’ with genomics, transcriptomics, epigenomics, proteomics and metabolomics to better enable a holistic approach to studying MDR (68-69). Since MDR is a complex phenotype, it makes sense to study genes, transcription, translation, proteins, metabolites and epigenetic factors that contribute to our

knowledge base. In addition, resources such as the Protein Data Bank (PDB) have reported the 3D structures of several transporters which has significantly aided drug discovery and development (<https://www.rcsb.org/>).

Despite challenges, advancements in the structural biology of ABC transporters and novel therapeutic strategies hold promise for overcoming MDR. Methods to determine or predict the structure of these ABC transporters can include X-ray crystallography, nuclear magnetic resonance (NMR), cryogenic electron microscopy (cryo-EM) and AlphaFold. Data from these studies have resulted in drug design that attempts to circumvent MDR through more potent inhibitors and drugs which are poor substrates of ABC transporters (24,27,70-73).

Future therapies may combine drug transporter inhibitors with other modalities such as immunotherapy, to enhance their efficacy while minimizing side effects. Overall, the outlook in cancer research is moving in a positive direction. With the emergence of more comprehensive datasets, there is lots of ground for new discoveries on MDR. Drugs are no longer limited to small molecules with the availability of monoclonal antibodies. Immunotherapies can enhance the efficacy of small molecule drugs. In addition, small molecule drugs can be given together in therapeutic regimens as combination chemotherapy. Chapter 2 will describe these big datasets in more detail focusing particularly on RNA sequencing and drug screening.

CHAPTER 2

COMPUTATIONAL DATABASES

Subsection 1: DrugBank

DrugBank is a comprehensive online resource that integrates detailed drug data with extensive information on drug targets and actions (74). DrugBank supports multiple applications, including *in-silico* drug discovery, drug design, drug docking and screening, drug metabolism prediction, drug interaction prediction and pharmaceutical education.

In 2006, the first version of DrugBank was released (74). Originally, DrugBank was developed to bridge the gap between clinically oriented drug resources and chemically oriented drug databases. It combines clinical information (drug action, absorption, distribution, metabolism, excretion, toxicity (ADMET)) with chemical information (structures, properties) in a single platform.

Given its focus on clinical and chemical information, DrugBank has a multi-audience focus. It was designed for pharmacists, clinicians, researchers and educators. Specifically, DrugBank provides detailed information on nomenclature, chemistry, structure, drug actions, pharmacology, pharmacokinetics, metabolism and drug-target interactions for each drug entry. Tables 1-3 display DrugBank retrieved information for the taxanes, anthracyclines, and vinca alkaloids. These drug classes are commonly used in cancer treatment, and most of them are well characterized through DrugBank.

As a database, DrugBank contains links to other databases. These include but are not limited to GenBank (NIH genetic sequence database) (75), UniProt (protein sequence and

Table 1. Taxane DrugBank Data. Physicochemical properties, ADMET parameters and clinical information.

	Paclitaxel	Docetaxel	Cabazitaxel
Brand Names	Abraxane Taxol	Docivyx Taxotere	Jevtana
Type	Small molecule	Small molecule	Small molecule
Average Weight	853.9061	807.8792	835.9324
Chemical Formula	C ₄₇ H ₅₁ NO ₁₄	C ₄₃ H ₅₃ NO ₁₄	C ₄₅ H ₅₇ NO ₁₄
Indication(s)	Sarcoma Lung cancer Ovarian cancer Breast cancer	Breast cancer Lung cancer Protstate cancer Gastric cancer Head and neck cancer	Prostate cancer
Mechanism of Action	Microtubule polymerization	Microtubule polymerization	Microtubule polymerization
Metabolism	CYP2C8 CYP3A4	CYP3A4 CYP3A5	CYP3A4 CYP3A5 CYP2C8
P-glycoprotein	Substrate	Substrate	Substrate

functional information database) (76), Protein Data Bank (3D structural data of large biological molecules) (70), ChEMBL (bioactive molecules with drug-like properties) (77), KEGG (bioinformatics resource) (78) and PubChem (79). This facilitates cross-referencing and extended research applications.

DrugBank has broad applicability and usefulness for a wide range of scientific fields, including pharmacogenomics, pharmacoproteomics, pharmacometabolomics and pharmacoconomics. DrugBank is frequently used by the research community, has been cited in numerous studies and is integrated into many international databases (80-83).

DrugBank continually evolves over time as evidenced by six versions of the database (74,84-88). Currently, DrugBank is at Version 6.0 with every update including more data fields, enhanced search tools and improved visualization capabilities. Additionally, these regular

Table 2. Anthracycline DrugBank Data. Physicochemical properties, ADMET parameters and clinical information.

	Doxorubicin	Daunorubicin	Epirubicin	Idarubicin
Brand Names	Adriamycin Doxil Myocet	Cerubidine Vyxeos	Elleence Pharmorubicin PFS	Idamycin
Type	Small molecule	Small molecule	Small molecule	Small molecule
Average Weight	543.5193	527.5199	543.5193	497.4939
Chemical Formula	C ₂₇ H ₂₉ NO ₁₁	C ₂₇ H ₂₉ NO ₁₀	C ₂₇ H ₂₉ NO ₁₁	C ₂₆ H ₂₇ NO ₉
Indication(s)	Leukemia Breast cancer Wilms tumor Neuroblastoma Soft tissue sarcoma Bone sarcoma	Leukemia	Breast cancer	Leukemia
Mechanism of Action	DNA intercalation ROS accumulation	DNA intercalation ROS accumulation	DNA intercalation DNA-TOP II complex stabilization DNA replication and transcription inhibition	DNA intercalation DNA-TOP II complex stabilization
Metabolism	NAPD(+) NADPH3 NADPH1			
P-glycoprotein	Substrate	Substrate	Substrate	Substrate

DrugBank updates are based on user feedback and advances in drug research and development (88).

DrugBank is designed to serve multiple audiences, including pharmacists, clinicians, researchers and educators. For drug nomenclature, chemistry and structure, DrugBank has information on drug names, synonyms, chemical structures and molecular formulas. For drug function and action, it includes data on mechanism of action, pharmacology, pharmacokinetics and metabolic properties. Additionally, DrugBank has extensive data on diseases targeted by

Table 3. Vinca Alkaloid DrugBank Data. Physicochemical properties, ADMET parameters and clinical information.

	Vinblastine	Vincristine	Vindesine	Vinorelbine
Brand Names		Marqibo Vincasar		
Type	Small molecule	Small molecule	Small molecule	Small molecule
Average Weight	810.9741	824.972	753.941	778.947
Chemical Formula	C ₄₆ H ₅₈ N ₄ O ₉	C ₄₆ H ₅₆ N ₄ O ₁₀	C ₄₃ H ₅₅ N ₅ O ₇	C ₄₅ H ₅₄ N ₄ O ₈
Indication(s)	Breast cancer Testicular cancer Lymphoma Neuroblastoma Sarcoma	Leukemia Lymphoma Wilm's tumor Neuroblastoma Sarcoma	Leukemia Lymphoma	Lung cancer Lymphoma Head and neck cancer Ovarian cancer Breast cancer
Mechanism of Action	Microtubule depolymerization	Microtubule depolymerization	Microtubule depolymerization	Microtubule depolymerization
Metabolism	CYP3A family	CYP3A family		CYP3A family
P-glycoprotein	Substrate	Substrate	Substrate	Substrate

drug and the proteins, genes and organisms involved. DrugBank has information on pharmacogenomics, metabolism and interactions by incorporating data on drug interactions (drug-drug, food-drug), ADMET properties (Absorption, Distribution, Metabolism, Excretion, Toxicity), pharmacogenomic data and pathways related to drug actions. Lastly, DrugBank is completely integrated with other databases on genetic sequencing (GenBank) (75), protein sequencing (UniProt) (76), large molecule 3D structures (Protein Data Bank) (70), drug-like properties (ChEMBL) (77), bioinformatics (KEGG) (78) and PubChem (79) among others (74).

The first version of DrugBank was published in 2006. DrugBank 1.0 contained nearly 90 data fields per drug entry. It provided detailed information on small molecule drugs (841 entries) and biotech drugs (113 entries). In general, DrugBank 1.0 focused on integrating data from multiple sources and making it searchable for various applications in drug discovery and education. DrugBank 1.0's main contribution was the database itself and the drugs within it

Table 4. DrugBank Data Entries. Expansion of DrugBank data through versions 1.0, 2.0, 3.0, 4.0, 5.0 and 6.0.

Number of	1.0	2.0	3.0	4.0	5.0	6.0
Data fields per DrugCard	88	108	148	208	215	
Search types	8	12	16	18	20	23
Illustrated drug-action pathways	0	0	168	232	319	404
Illustrated drug metabolism pathways	0	0	0	53	64	2,721
Drugs with metabolizing enzyme data	0	0	762	1,037	3,859	
Drug metabolites with structures	0	0	0	1,239	1,360	3,037
Drug-metabolism reactions	0	0	0	1,308	1,530	3,703
Drugs with drug transporter data	0	0	516	623	1,954	3,408
Drugs with taxonomic classification information	0	0	0	6,713	7,387	12,723
Inferred SNP-associated drug effects	0	0	0	0	5,993	
Directly studied SNP-associated drug effects	0	0	114	201	324	
Drugs with patent/pricing/manufacturer data	0	0	1,208	1,450	1,820	
Food-drug interactions	0	714	1,039	1,180	1,195	2,475
Drug-drug interactions	0	13,242	13,795	14,150	365,984	1,413,413
ADMET parameters	0	276	890	6,667	6,700	
QSAR parameters per drug	5	6	14	23	23	
Drugs with drug-target binding constant data	0	0	0	791	1,563	
Drugs with experimental NMR data	0	0	0	306	922	1,822
Drugs with experimental MS spectra	0	0	0	384	2,521	2,888
Drugs with chemical synthesis information	0	38	38	1,285	1,584	
Approved small molecule drugs	841	1,344	1,424	1,552	2,110	2,751
Approved drugs with product ingredient structures	0	0	0	474	1,551	4,030
Biotech drugs	113	123	132	284	555	1,601
Nutraceutical drugs	61	69	82	87	97	134
Withdrawn drugs	0	57	68	78	209	317
Illicit drugs	0	188	189	190	202	205
Experimental drugs	2,894	3,116	5,210	6,009	4,964	6,722
Investigational drugs	0	0	0	1,219	4,501	6,231
All drug targets	2,133	3,037	4,326	4,115	4,563	4,939
Approved-drug enzymes/carriers	0	0	164	245	479	526
All drug enzymes/carriers	0	0	169	253	497	556
External database links	12	18	31	33	35	
Total drug product pill images	0	0	0	0	3,600	
Linked drug indications	0	0	0	0	3,024	3,820
Clinical trials	0	0	0	0	245,356	464,870

(small molecule, biotech, nutraceutical, experimental). Table 4 details the addition of new data types and expansion of current data types from DrugBank Version 1.0 to 6.0 (74,84-88).

The second version of DrugBank was published in 2008 (84). DrugBank 2.0 was expanded to include 60% more FDA approved drugs and a significant increase in experimental drug data. It introduced new data fields such as food-drug interactions, drug-drug interactions and experimental ADMET data. This reflects DrugBank's widespread appeal to clinicians, patients and the public. In addition, new entries were added on chemical synthesis information, withdrawn drugs and illicit drugs. Lastly, DrugBank 2.0 had improved search capabilities and added new tools for data querying and viewing (84).

The third version of DrugBank was published in 2011 (85). DrugBank 3.0 added more than 40 new data fields per drug entry, including data on drug pathways, transporters, metabolites, pharmacogenomics and adverse drug responses. It also introduced new tools for querying and viewing drug pathways and interactions. This update emphasized 'omics' applications which makes the database more useful for pharmacy-related fields such as pharmacogenomics, pharmacoproteomics, pharmacometabolomics and pharmacoeconomics research. In addition, DrugBank 3.0 expanded the number of entries for established data fields and incorporated new data fields such as drug enzymes and carriers, and single nucleotide polymorphism (SNP) associated drug effects. It focused on expanding data related to drug metabolism, ADMET and Quantitative Structure-Activity Relationship (QSAR). DrugBank 3.0 enhanced capabilities for predicting and characterizing xenobiotic metabolism, pharmacokinetics and pharmacodynamics (85).

The fourth version of DrugBank was published in 2014 (86). DrugBank 4.0 included >1,200 drug metabolites which further supports research in drug metabolism and

pharmacokinetics. Additionally, it introduced illustrated drug metabolism pathways, drug metabolite structures, drug metabolism reactions, drug-target binding constant data, experimental NMR data and MS spectra and investigational drugs. DrugBank 4.0 increased the number of data entries for drug metabolizing enzyme data, drug transporter data, food-drug and drug-drug interactions, ADMET parameters, chemical synthesis information, approved small molecule drugs and drug enzymes/carriers (86).

The fifth version of DrugBank was published in 2018 (87). DrugBank 5.0 introduced more sophisticated search tools and enhanced data integration with other databases. It also added new data entries for drug information on drug metabolites, drug interactions and pharmacogenomics. DrugBank 5.0 further improved the database's user interface and usability which makes it more accessible to a broader audience. It increased the drugs with metabolizing enzyme data and drug transporter data. Lastly, DrugBank 5.0 added categories on drug indications (3,024 entries), clinical trials (245,356 entries) and drug product pill images (3,600 entries) (87).

The sixth version of DrugBank was published in 2024 (88). DrugBank 6.0 further expanded the scope of the database with more data fields and improved data accuracy. It enhanced data visualization tools, including new features for exploring drug pathways, interactions and targets. In general, most data fields had increased entries for illustrated pathways, metabolizing enzyme data, drug transporter data, drug interactions (food-food, drug-food), approved drugs (small molecule, biotech, nutraceutical), non-approved drugs (withdrawn, illicit, experimental, investigational), drug enzymes and carriers, clinical trials and drug indications. Overall, DrugBank 6.0 has a continued focus on supporting a wide range of scientific and clinical applications from drug discovery to personalized medicine (88).

Since its initial release nearly 20 years ago, DrugBank has progressively increased its data coverage and depth by adding more drug entries, data fields and integration with other databases. The database has continuously enhanced its querying capabilities and data visualization tools which make it a powerful resource for researchers and clinicians. With each new version, DrugBank has expanded its application to more fields including ‘omics’ research, personalized medicine and drug safety. The development of DrugBank has been heavily influenced by user feedback which led to numerous updates that align with the needs of its user base. DrugBank’s regular updates ensure it evolves with major clinical and chemical developments and remains a valuable resource.

Subsection 2: CTRP, GDSC and PRISM

The Cancer Therapeutics Response Portal (CTRP) was developed to systematically link genetic and lineage features of cancer cell lines (CCLs) with small molecule sensitivities to identify novel cancer dependencies and potential therapeutic targets (89). CTRP profiles the sensitivity of 242 CCLs to an ‘Informer Set’ of 354 small molecules including FDA approved drugs, clinical candidates and probes targeting diverse cellular processes. Specifically, CTRP focuses on identifying drug dependencies which can be targeted, including dependencies induced by specific genomic alterations. Lastly, CTRP aims to be a dynamic, evolving resource that integrates additional data and analyses over time (89).

The Genomics of Drug Sensitivity in Cancer (GDSC) database was developed to facilitate the discovery of molecular biomarkers of drug response by linking cancer cell line drug sensitivity data with extensive genomic data (90). GDSC contains drug sensitivity data for ~75,000 experiments which covers responses to 138 oncology drugs across ~700 cancer cell lines. It integrates this cell line drug sensitivity data with large genomic datasets, including

somatic mutations, gene amplifications and deletions, tissue types and transcriptional data from the Catalogue of Somatic Mutations in Cancer (COSMIC) database. Overall, GDSC was designed to identify molecular markers that can predict cancer response to various therapies (90).

The Profiling Relative Inhibition Simultaneously in Mixtures (PRISM) database was generated to improve the throughput and accuracy of drug sensitivity screening by using a pooled cell line approach (91). PRISM utilizes DNA barcoding and next-generation sequencing to screen thousands of compounds against large, diverse cell line pools at the same time. It focuses on discovering cancer vulnerabilities and potential drug combinations by noting the effects of treatments across multiple cancer cell lines in parallel. In general, PRISM’s goal is to increase the scalability of drug screening and facilitate the identification of biomarkers linked to drug response (91).

Table 5. Drug Screening Databases. Comparison of CTRP, GDSC and PRISM drug screening platforms (original releases).

	CTRP	GDSC	PRISM
Cancer cell lines	242	700	578
Approved or clinical trial drugs	89	138	3,350
Probes	265	0	0
Tool compounds	0	0	1,168
Drug sensitivity assay	CellTiter-Glo	CellTiter-Glo	Cell barcoding
Drug sensitivity metric	AUC	AUC	AUC
Drug concentrations	8	9	8

Table 5 outlines the major similarities and differences between these drug screening databases. CTRP, GDSC and PRISM aim to identify molecular biomarkers and cancer vulnerabilities that can predict drug sensitivity and guide targeted therapy development while taking different approaches. All three databases utilize high-throughput screening techniques to assess drug responses in cancer cell lines by integrating these data with extensive genomic

profiling. In addition, CTRP, GDSC and PRISM integrate this drug sensitivity data with genomic features such as mutations, copy number variations and gene expression profiles to identify correlations and potential therapeutic targets (92). The emphasis on linking specific genetic alterations to drug sensitivity can facilitate the discovery of novel cancer dependencies and subsequent therapeutics.

Lastly, the data from these projects is made public and available free to researchers with user friendly interfaces and tools to query, visualize and analyze the information. CTRP, GDSC and PRISM platforms offer downloadable datasets and tools for analyzing drug response data and the associated genomic features (89-91).

Although CTRP, GDSC and PRISM share similar goals, each database takes a slightly different approach. CTRP uses a more extensive set of small molecules (354) including FDA approved drugs, clinical candidates and probes to model a broader range of cellular processes. Data on drug sensitivity is collected using a traditional format by assessing responses in 242 CCLs to generate dose-response curves and compute metrics like area under the curve (AUC). Lastly, CTRP focuses on identifying known and novel oncogene-induced dependencies by integrating genetic and lineage features (89).

Alternatively, GDSC conducts drug sensitivity screening on a smaller subset of 138 oncology drugs across ~700 cancer cell lines. This database utilizes comprehensive genomic datasets from the COSMIC database and applies statistical approaches like multivariate analysis variance (MANOVA) and elastic net regression to identify genomic markers of drug response. In contrast to CTRP, GDSC focuses more on therapeutic biomarker discovery and integrating large datasets for preclinical validation (90).

Finally, PRISM uses a unique pooled cell line approach where cancer cell lines are barcoded and pooled together for drug screening. It employs next-generation sequencing to measure relative cell survival in response to treatments which enables simultaneous screening of thousands of compounds against large cell line panels. PRISM also attempts to improve throughput and scalability which reduces the cost and time needed for drug sensitivity testing (91).

The datasets vary widely in the number of compounds tested, compound classification and cancer cell lines covered. CTRP offers a smaller, more focused dataset targeting specific cancer dependencies and was designed to be a “living resource” which is updated continually with new data and analyses. GDSC encompasses a larger dataset (75,000 experiments) with a focus on integrating detailed genomic data to facilitate therapeutic biomarker discovery with an ongoing expansion. Lastly, PRISM is centered on high throughput drug screening using pooled cell lines for improved efficiency and scalability in identifying drug responses across diverse cancer types (89-91).

Each dataset contributes in the way of technological innovation. CTRP leverages traditional high-throughput screening techniques but focuses on integrating diverse datasets for comprehensive analysis of drug sensitivity and genomic dependencies. Instead, GDSC emphasizes the use of sophisticated statistical modeling and genomic data integration to uncover biomarkers. Notably, PRISM innovates by using DNA barcoding and sequencing technology to achieve simultaneous drug screening across multiple cancer cell lines which increases throughput and decreases cost (89-91).

To summarize, CTRP, GDSC and PRISM have common goals of understanding cancer drug sensitivities and identifying biomarkers for therapy. However, they have different

technological approaches, methodologies and general scope. CTRP offers a flexible, evolving platform for analyzing small molecule dependencies linked to cancer genomics. GDSC has the most extensive dataset for genomic correlations with drug sensitivity which is focused on therapeutic biomarker discovery. PRISM enhances the efficiency and scalability of drug screening. This facilitates a faster identification of potential therapies and drug combinations (89-91).

Subsection 3: CCLE

The Cancer Cell Line Encyclopedia (CCLE) was created as a comprehensive resource which connects the genomic features of ~1,000 cancer cell lines with drug sensitivity data (92). It facilitates the identification of genetic, lineage and gene expression-based predictions of drug sensitivity which facilitates the development of personalized cancer therapies. CCLE supports predictive modeling of oncology drug sensitivity which advances the field of precision oncology.

In its original version, CCLE encompassed the characterization of 947 human cancer cell lines which cover 36 tumor types (93). Data includes gene expression, chromosomal copy number variations and mutational status of >1,600 genes determined by targeted massively parallel sequencing. In addition, CCLE profiled 24 oncology drugs across 479 cell lines which yielded eight-point dose-response curves. CCLE uses machine learning models, including elastic net regression, to correlate the genomic features with drug sensitivity to identify potential biomarkers (93).

In its updated version, CCLE expanded its database to include additional genomic characterizations such as RNA sequencing, whole exome and whole genome sequencing, DNA methylation, histone modification, microRNA expression and reverse-phase protein array data for >1,000 cell lines. It also incorporated data from short hairpin RNA (shRNA) knockdowns,

CRISPR-Cas9 knockouts and metabolite abundance to identify potential therapeutic targets and biomarkers (92).

Overall, CCLE’s goal is to provide a preclinical framework to predict drug responses in cancer by leveraging the molecular and genetic data of a broad range of cancer cell lines. It supports the discovery of novel genetic markers and dependencies that can inform therapeutic strategies. In addition, CCLE offers an extensive repository for cancer research that can be used to study genetic variants, candidate targets and effects of small molecule and biological therapeutics. It integrates several datasets to facilitate research into gene function, cancer progression and therapeutic intervention. As a database, CCLE is publicly, globally accessible for researchers which promotes collaboration and data sharing. Thus, it contributes to global cancer research efforts by providing data that is easily available and continuously updated (92-93).

Table 6. Cancer Cell Line Database. CCLE cancer cell line sequencing, profiling and arrays.

Analysis	CCLE CCLs
Total Cancer cell lines (CCLs)	1,072
RNA sequencing (RNA-seq)	1,019
Whole exome sequencing (WES)	326
Whole genome sequencing (WGS)	329
Reverse-phase protein array (RPPA)	899
Reduced representation bisulfite sequencing (RRBS)	843
MicroRNA expression profiling	954
Global histone modification profiling	897

Table 6 lays out the current data in CCLE and genetic characterization of cancer cell lines. Currently, CCLE offers comprehensive genomic data, including single nucleotide polymorphism (SNP) arrays, whole

genome sequencing (WGS), whole exome sequencing (WES), RNA sequencing, DNA methylation and chromatin profiling. It also encompasses analyses of structural variants, gene fusions and mutational signatures linked to cancer progression. It contains drug sensitivity data for 24 oncology drugs including dose-response curves and machine learning-based predictive

models. Lastly, it has data on shRNA knockdowns and CRISPR-Cas9 knockouts to correlate gene dependencies with drug responses (92).

As a database, CCLE is well integrated across multiple omics layers through microRNA expression, histone modification and protein expression profiles. Finally, CCLE is a user-friendly online portal for researchers to query, download and visualize data. CCLE is linked with the Cancer Dependency Map Portal (DepMap Portal) for easy access to gene dependency and compound profiling data (92-94).

In addition to CCLE, The Cancer Genome Atlas (TCGA) is another large-scale genomic dataset. Specifically, TCGA contains the molecular characterization of >20,000 primary cancer samples across 33 cancer types (95). Since it focuses exclusively on primary tumors, TCGA is a parallel resource to CCLE for studying cancer genomics. The combination of these genomic and drug screening databases facilitates work toward quantifying MDR in cancer.

CHAPTER 3

QUANTITATIVE METRICS

Subsection 1: Multidrug Resistance Overview

Drug response in cells is complex. Back in the 1800s, Paul Ehrlich worked on the chemical composition of drugs and their mechanism of action (96). He worked on anti-toxins and wanted to figure out how to make anti-toxins 100% neutralizing to the toxins but not to other cells. Ehrlich studied the idea of complementarity where an anti-toxin binds to the target toxin but not to anything else. This led Ehrlich to study enzyme-substrate affinity and gave way to his work on receptors. He then proposed the ‘lock and key’ model for receptors which linked the chemical structure of compounds to pharmacological activity. Essentially, the lock is the enzyme, and its substrate is the key which fits into a specific binding pocket within the enzyme. This fit enables the compound’s pharmacological activity (97).

Ehrlich proposed the concept of receptor theory, but Archibald Hill made it quantitative. In the early 1900s, Archibald Hill introduced the Hill equation to describe the interaction between hemoglobin and oxygen (98). After one oxygen binds to hemoglobin, it becomes easier for more oxygen molecules to bind other sites on the hemoglobin as the active sites change conformation to increase the likelihood of additional binding. This is depicted by the Hill equation and describes how drugs bind to their targets: $\% \text{ binding} = \frac{[\text{Drug}]}{([\text{Drug}] + K_d)}$. As the intracellular binding site becomes saturated with substrate, the curve for binding produces a sigmoidal shape (99).

The Hill equation models a drug binding directly to its target protein with the dissociation rate constant, K_d , as a measure of binding affinity. Once an enzyme is saturated, it leads to dose response curves where the excess substrate is bound to all available enzymes. In cells, the % binding can be approximated to the effective concentration 50 (EC_{50}) which measures the concentration of drug needed to achieve 50% cell death (Figure 5A and 5B). In the Hill equation, this assumes that all drug inside the cell becomes bound to the intracellular target.

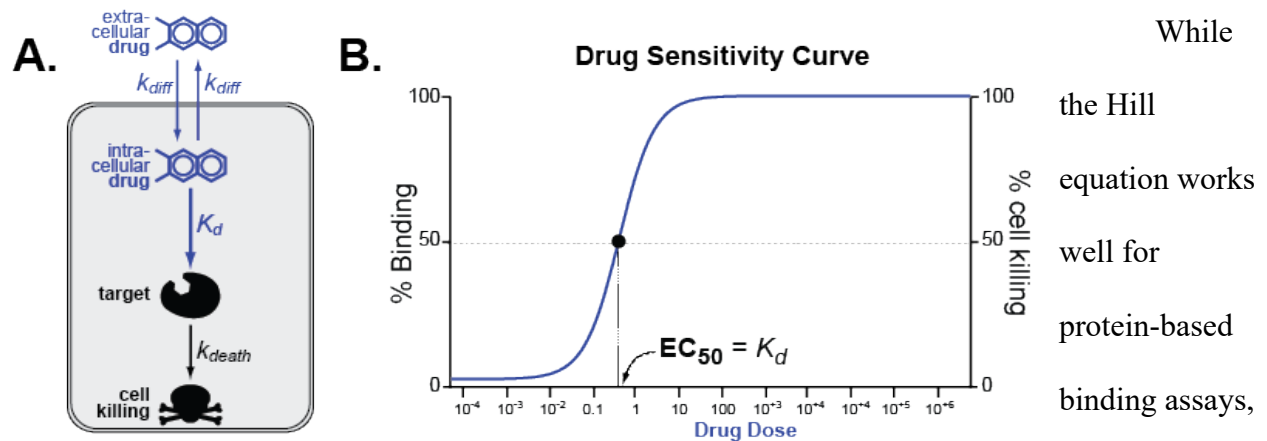


Figure 5. Mathematics of Drug Dose Response. The EC_{50} can be approximated to the K_d in normal tissues. (A) Drug diffuses into cells where the $[drug]_{in}$ equals the $[drug]_{out}$. Drug binds to the intracellular target measured through the K_d . Bound drug causes cell death measured through the k_{death} . (B) The % binding to the intracellular target can be approximated to the % cell killing in a dose response curve.

While the Hill equation works well for protein-based binding assays, it is incomplete for cells. When the Hill equation is

applied to cells, there are several implicit assumptions made which can be inaccurate. One key assumption is that the drug concentration inside the cell equals the drug concentration outside the cell ($[drug]_{in} = [drug]_{out}$), so the EC_{50} can be approximated to the K_d meaning all substrates bound to the target are linked to its effect. In most cases, this is true, but enzymes such as drug pumps change the equilibrium, so the $[drug]_{in} \ll [drug]_{out}$.

Xenobiotic enzymes defend the body from diverse toxins and therefore, do not fit the 'lock and key' concept of substrate specificity. They help the human body eliminate, detoxify

and metabolize drugs. Thus, most xenobiotic enzymes are expressed in the liver, intestines, kidneys, lungs, blood and brain. The largest class of xenobiotic enzymes is the Cytochrome P450 (CYP450) family which are mainly involved in the first phase of metabolism (100). The goal of Phase I drug metabolism is to create a polar, water soluble metabolite through oxidation, reduction or hydrolysis. The product of Phase I leads to Phase II drug metabolism in which metabolites are conjugated to charged species through glucuronidation, sulfation, glutathione conjugation, methylation and acetylation. The addition of these ionized groups makes the metabolites more water soluble and higher molecular weight, so they are more easily excreted from the body (101-102).

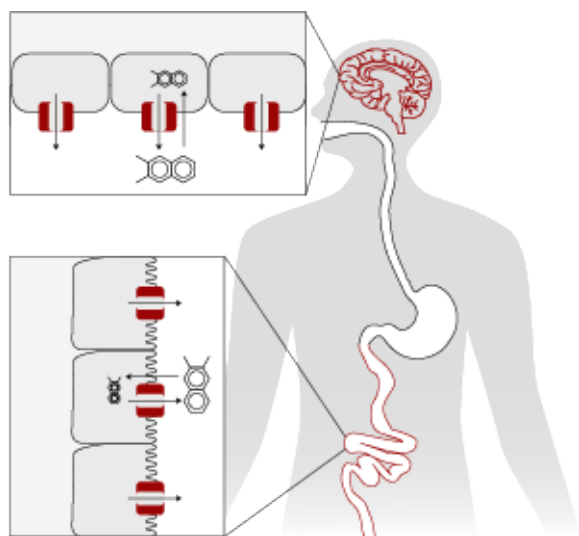


Figure 6. Pgp Normal Expression in Tissues. Pgp is typically expressed in tissues with pharmacokinetics and barrier functions such as the brain, intestines, liver and kidneys.

However, CYP450 enzymes have been implicated for their role in multidrug resistance (MDR). CYP450 enzymes are not only expressed in tissues but within individual cells. In cells, they metabolize a fraction of drug when it enters the cell. This is a protection mechanism to prevent high levels of drug from accumulating and causing toxicity (103-105).

Additionally, a third group of xenobiotic enzymes are the drug transporters. These enzymes also protect the tissues and cells by pumping out

drug. Drug transporters have an important physiological role and are highly expressed in barrier tissues and tissues involved in drug pharmacokinetics in the body (Figure 6). Tissues with high

amounts of drug transporters include the brain, intestines, colon, liver, kidneys and testes (105-110).

The most notable group of drug transporters are the ATPase Binding Cassette (ABC) transporters (30). ABC transporters encompass subfamilies of which ABC subfamilies B, C and G are best known for conferring drug resistance. *ABCB1* is the gene for Permeable glycoprotein (Pgp), an extensively studied drug transporter in the context of cancer MDR (111).

Pgp defies standard pharmacologic theory because it pumps out various substrates (112). This is from Pgp's globular binding pocket which can accommodate many different chemical structures of drugs. MDR enzymes typically follow pseudo-first order reaction kinetics (113). Since Pgp can pump out many different substrates, it has a large K_m because its affinity is not very high for any one substrate. Thus, we can assume that the $[drug]_{in}$ is much lower than the K_m which means we can approximate the EC_{50} to the K_m in the linear regime of the reaction.

As a promiscuous enzyme, Pgp has been described as a vacuum cleaner by "sucking up" drug from the cell membrane and pumping it out (114). Pgp is the first ABC transporter discovered and accordingly, the drug pump most studied in the scientific literature (85). As a family, ABC transporters are promiscuous and accommodate many drugs though they have preference for different substrates which underlies their physiological role. The description of drug pumps as "vacuum cleaners" is perhaps a more accurate depiction as they pump out a variety of drugs and biochemical molecules (114). This contrasts with Ehrlich's description of enzyme receptors through a 'lock and key' model where one substrate fits into one enzyme (96).

In the 1900s, Michaelis-Menten enzyme kinetics came from the study of a reaction yielding fructose and glucose from sucrose catalyzed by invertase (115). For this reaction, Michaelis and Menten discovered the formation of an enzyme-substrate complex by measuring

the velocity of the reaction as a function of sucrose concentration. Michaelis-Menten enzyme kinetics are different from the Hill equation in that they incorporate reaction velocity as a function of enzyme concentration and substrate turnover (116).

The output of the Hill equation is a measure of binding affinity of a substrate for an enzyme (Equation 1). The Michaelis-Menten equation expands on the Hill equation by changing the K_d to K_m (Equation 2). The K_m is the substrate concentration at which the enzyme reaction is half-maximal, so a smaller K_m indicates greater binding affinity. The Michaelis-Menten equation defines the maximum velocity, V_{max} of the enzyme-catalyzed reaction as a function of enzyme concentration, $[E]$ and rate of substrate turnover, k_{cat} (Equation 3). Since a greater enzyme concentration and substrate turnover increases the maximum reaction velocity, these factors contribute to an overall greater reaction velocity (Equation 4).

Equation 1: % binding = $[Drug] / ([Drug] + K_d)$

Equation 2: velocity = $[Drug] / ([Drug] + K_m)$

Equation 3: $V_{max} = [E] * k_{cat}$

Equation 4: velocity = $(V_{max} * [Drug]) / ([Drug] + K_m)$

As with the Hill equation, there are some key assumptions made in the context of modeling MDR with drug transporters. First, the contribution of enzymes to MDR is additive with each enzyme contributing independently to flux. Second, Pgp is a promiscuous enzyme with a high K_m for multiple drugs, so the K_m is much larger than the $[drug]_{in}$. Third, drug influx is impacted by diffusion only, so $[drug]_{in} = [drug]_{out}$ at steady state (115).

Under first order conditions ($[substrate] < K_m$), the membrane transport rate (k_{efflux}) is expected to be the $k_{cat} * [Transporter] / K_m$ (117-118). This assumption is commonly used for membrane transporters and is consistent with clinical pharmacokinetics where xenobiotic

enzymes are assumed to act under first order conditions clinically (113). Thus, Michaelis-Menten enzyme kinetics can be thought of as a linear relationship where $y = \text{slope} * x$. In this linear relationship, y is the efflux rate (k_{efflux}), slope is $(k_{\text{cat}} / K_m) / k_{\text{diff}}$ and x is MDR expression ($[E]$). This corresponds to the change in drug EC_{50} . If we assume pseudo-first order conditions, then EC_{50} and $[E]$ are expected to be linear (Figure 7) (119).

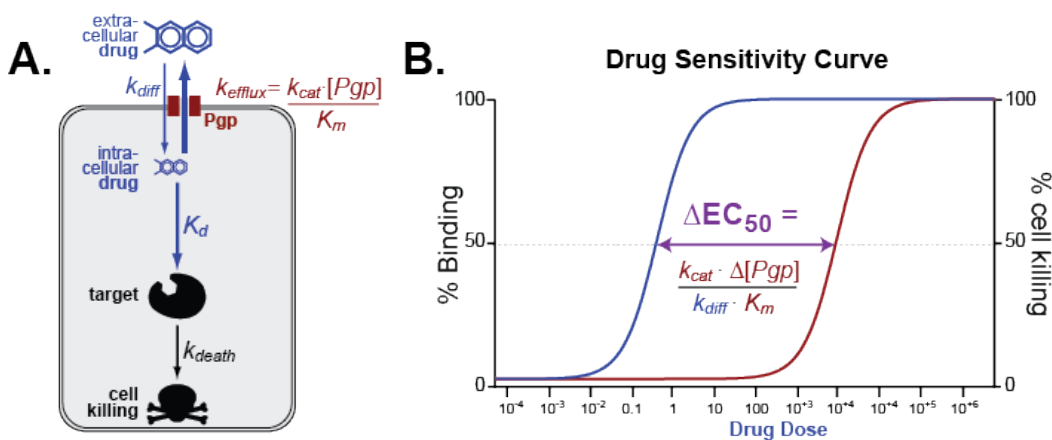


Figure 7. Drug Dose Response in MDR. Multidrug resistant cancer cells increase the EC_{50} . (A) Multidrug resistant cancer cells have increased Pgp expression. Pgp increases drug efflux, so $[\text{drug}]_{\text{out}} \gg [\text{drug}]_{\text{in}}$ measured through the k_{efflux} . Less drug is available to bind to the intracellular target and cause cancer cell death. (B) Pgp expression shifts the EC_{50} right because a larger drug dose is required to achieve 50% binding and cell killing.

This decreased drug potency and resulting EC_{50} shift is an indication of the MDR phenotype. Fortunately, we have data on this phenotype from new databases such as DrugBank, CTRP, GDSC, PRISM and CCLE which were described extensively in Chapter 2. To bridge these *in-vitro* databases with clinical data, we examined 34 most FDA-indicated chemotherapies and *in-vitro* data from the Cancer Dependency Map Portal (<https://depmap.org/portal>,94). Our analysis demonstrated a correlation between biomarkers (direct binding, metabolism, transport, DNA repair) and drug sensitivity (results are shown in more detail below). Further analysis

showed that biomarker RNA expression is directly correlated with drug EC_{50} . Thus, a drug's EC_{50} change can be modeled by a kinetic ratio in MDR cancers.

There are increasing efforts to digitize raw data from primary literature references which give us the opportunity to compare MDR phenotypes and kinetic parameters across primary literature for the first time. Relevant examples for our quantitative analysis include BRENDA, ChEMBL and DrugBank (77,85,120). Specifically, BRENDA is an enzyme repository for information on enzyme biochemistry, structure, kinetics, function etc. (brenda-enzymes.org/). ChEMBL is a database for information on bioactive molecules with information on bioactivity and chemical properties (ebi.ac.uk/chembl/). DrugBank is a database with information on approved drugs including indication, mechanism, pharmacokinetics and pharmacodynamics (go.drugbank.com/). For BRENDA and ChEMBL, their goal is to bridge genomics with enzymes and drug-like molecules. DrugBank provides information on enzymes and chemistry for already approved drugs through the FDA and foreign regulatory agencies.

BRENDA is useful for MDR kinetic parameters such as k_{cat} and K_m . The BRAunschweig ENzyme DAtabase (BRENDA) was founded in 1987 at the German National Research Centre for Biotechnology as an enzyme information data system (120). The need for a systematic collection of enzyme information for genomic interpretation and field application underlies BRENDA. BRENDA was developed to provide more information on gene products and enzymes to match the increasing projects on genome sequencing. When BRENDA was originally published, it contained data from >46,000 primary literature references with data from >40,000 different enzymes. Specifically, BRENDA includes information on enzyme nomenclature, enzyme structure, enzyme-ligand interactions, functional parameters, molecular properties, organism-related information and bibliographic data (120).

In the 2020s, BRENDA has evolved to include >5 million data from 90,000 enzymes across 13,000 organisms from 157,000 primary literature references (121). Additionally, BRENDA now offers enzyme pathway maps covering metabolic pathways and biochemical processes. Viewers can see chemical reactions and enzyme-ligand information within the pathway maps. Currently, each enzyme has its own Enzyme Summary Page which gives an overview of all available information for it within BRENDA. It also incorporated a new tool which predicts the intracellular localization of each enzyme given its function (121).

To better understand BRENDA, we extracted k_{cat} and K_{m} values from this database and augmented this source with manual curation of additional literature. We wanted to use BRENDA to better understand Pgp as a “vacuum cleaner” model more quantitatively (114). So, we searched for primary literature references with data on K_{m} and k_{cat} values for Pgp. This analysis produced 137 entries including 47 different compounds with publications from 1995 to 2022. The average k_{cat} was 1.29 seconds⁻¹ and K_{m} was 154.88 μM . Our data ranged from 0.0139 to 1040 μM for the K_{m} and 0.7 to 3.3 seconds⁻¹ for the k_{cat} . There was significantly more data on K_{m} than k_{cat} which reflects more scientific focus on K_{m} as a metric for studying enzyme kinetics.

By overlaying the Pgp manual curation dataset with BRENDA for K_{m} and k_{cat} , the wide variability for these enzyme kinetics values is apparent. Even for the same substrate, there can be wide variety in the K_{m} and k_{cat} which can be traced to different experimental platforms and conditions (Figure 8). Figure 8A shows literature reported k_{cat} and K_{m} values for Pgp (pink) vs enzymes in BRENDA (gray). There is no agreement in the scientific literature on a single value for these enzyme kinetics parameters although there is major overlap among the reported values.

Figure 8B displays the organisms within the Pgp manual curation dataset and average values for *ABCB1* k_{cat} and K_{m} . As shown, *Homo sapiens* (humans) have highest average k_{cat} and

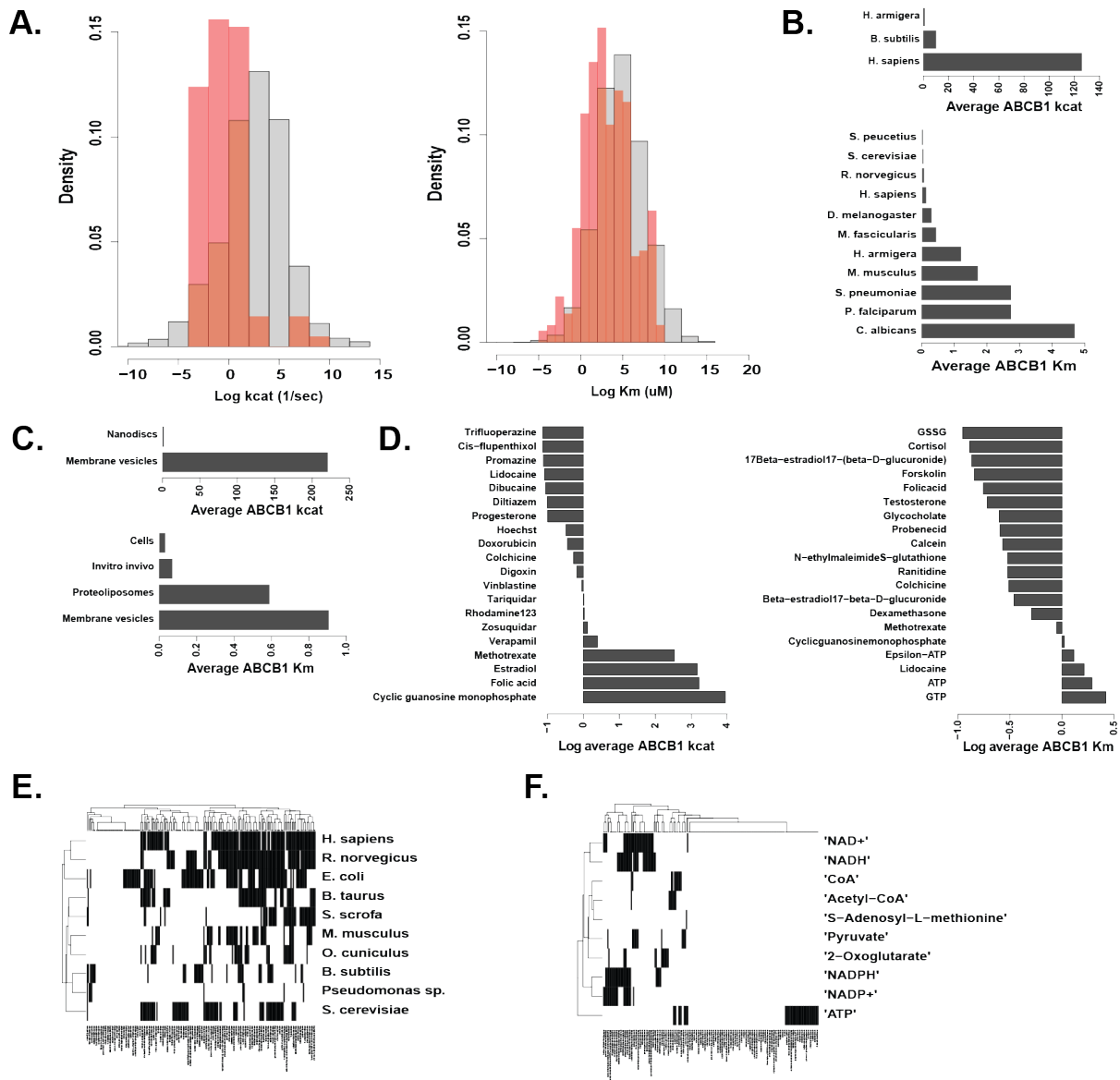


Figure 8. BRENDA Enzyme Kinetics Data. The BRENDA database offers enzyme information across organism, platform and compound. (A) Literature on Pgp reflects variability in reported enzyme kinetics values for k_{cat} and K_m (Pink: Pgp manual curation, Gray: BRENDA all enzymes). (B-D) Inconsistencies in enzyme information can be attributed to intrinsic differences in experimental conditions with organisms, platforms and compounds used. (E-F) BRENDA has current gaps in enzyme information across organism and compound.

Candida albicans (yeast) have the highest average K_m . Among the various experimental platforms used to study Pgp *in-vitro*, membrane vesicles yielded the highest average k_{cat} and K_m

(Figure 8C). This is likely due to differences in Pgp functionality once purified and reconstituted whether in membrane vesicles, liposomes or nanodiscs. In addition, there are many choices for substrates to study Pgp including inhibitors (Verapamil, Tariquidar, Zosuquidar), fluorescent dyes (Hoechst, Calcein, Rhodamine123), oncology drugs (Doxorubicin, Vinblastine), and nucleotides (ATP, GTP) among others. Thus, the reported k_{cat} and K_m values by compound is widespread since Pgp can bind vastly differently to a spectrum of compounds based on molecular weight, chemical structure etc. (Figure 8D).

Even though BRENDA is a comprehensive database, it still has gaps in studies. To illustrate this, the top ten organisms (Figure 8E) and top ten compounds (Figure 8F) in BRENDA were compared to the top 200 BRENDA enzymes by K_m values. For each organism-enzyme pairing and compound-enzyme pairing, if there are any reported K_m values within BRENDA, the pairing is black. But if there are no reported K_m values within BRENDA, the pairing is white. As demonstrated, there are gaps in our understanding of kinetics for specific enzymes in organisms and in compounds. But the knowledge gap is much more pronounced in our understanding of enzyme kinetics regarding compounds. This indicates that variation in enzyme kinetics is more widely thought about in terms of the organism. Overall, the widespread variability in organism, experimental platform and compound contributes to the disagreement on enzyme kinetics values in the scientific literature. As a drug transporter, there are many avenues for studying Pgp functionality and substrates.

With this raw K_m and k_{cat} data in hand, we next examined the current largest database documenting MDR-substrates available. BRENDA focuses on enzymes generally, but we wanted to narrow our focus to enzymes involved in MDR. Thus, we turned to DrugBank, a database developed to bridge gaps between clinically oriented drug resources and chemically

oriented drug databases. Originally, DrugBank combined clinical information (drug actions, pharmacology) with chemical information (structures, properties) in a single platform. It was tailored to pharmacologists, medicinal chemists and pharmacists. It was first released in 2006 and since then, has released five updated versions with enhanced data compilation, visualization, application etc. (74,84-88).

The 2011 version (DrugBank 3.0) added data on drug pathways, transporters, metabolizing enzymes, pharmacogenomics and adverse drug reactions (85). The data on transporters and metabolizing enzymes stems from scientific literature curation which introduces experimental variability. So, for transporters and metabolizing enzymes, DrugBank defines substrates in a binary way by assigning 1's to substrates and 0's to non-substrates (85). This variability is like BRENDA, so DrugBank probably used this classification method as a compromise because DrugBank curators could not find a consensus for K_m or k_{cat} values.

DrugBank has information on 63 xenobiotic enzymes. Since we are most interested in oncology drugs, we created a binary heatmap for MDR enzyme-drug pairings (Figure 9). In the binary heatmap, black indicates a substrate and white indicates a non-substrate according to DrugBank definitions. From the data, most current knowledge of MDR genes is centered on *ABCB1* which is the gene for Pgp. Thus, we focused our efforts on Pgp in the broader context of understanding MDR quantitatively (<https://go.drugbank.com/>).

Subsection 2: Potential for Functional Scoring

Clearly, DrugBank is a solid start to consolidating our knowledge on MDR but still has major gaps. Due to inconsistencies with MDR studies, a new metric is needed that has the potential for functionally scoring drugs by substrate specificity. Since substrate specificity is determined by gene expression and enzyme kinetics, we focused on the Cancer Cell Line

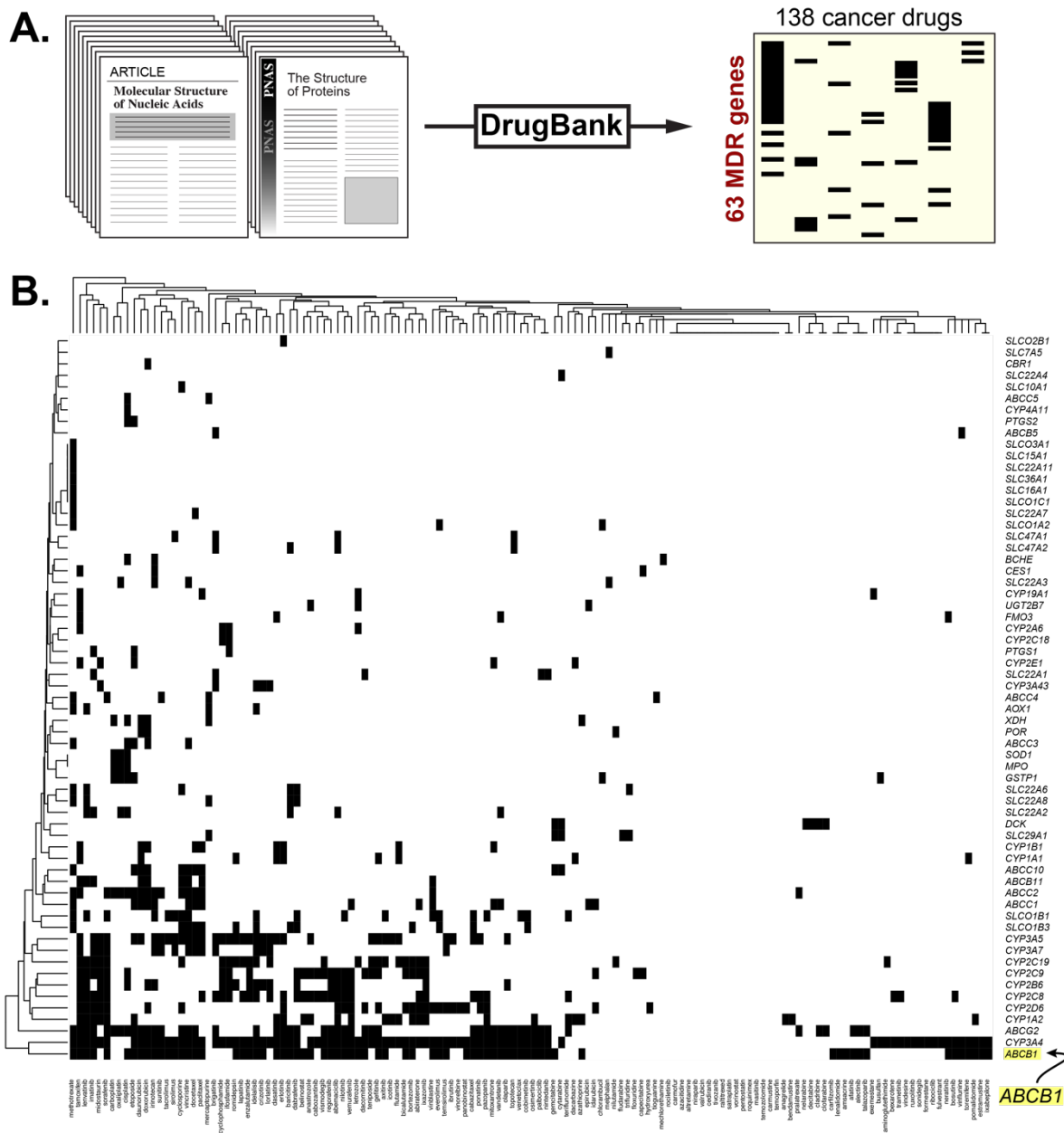


Figure 9. DrugBank MDR Genes and Drugs. DrugBank data on 63 MDR genes and 138 drugs. (A) DrugBank data is derived from the scientific literature. Sixty-three MDR genes representing ABC and SLC transporters and CYP450 metabolism were paired with 138 FDA approved oncology drugs. (B) Most current knowledge of MDR genes from the scientific literature is on *ABCB1*, the gene for Pgp.

Encyclopedia (CCLE) and Profiling Relative Inhibition Simultaneously in Mixtures (PRISM) databases which encompass both datasets across 479 cancer lines (91-92).

CCLF was generated from a collaboration between the Broad Institute out of MIT and Harvard and Novartis Institutes for Biomedical Research (93). CCLF covers the genetic characterization of ~1,000 cancer lines and has a plethora of data types including DNA, mRNA, protein, metabolites etc. We are interested in mRNA data specifically because Pgp and other xenobiotic enzymes are regulated at the RNA level by transcription factors (122).

We chose to use mRNA because it is generally accepted that xenobiotic enzyme expression is regulated at the transcriptional level (123). For example, the Pregnane X Receptor (PXR) is one transcription factor which is activated after drug binding and localized in the nucleus. PXR increases transcription of *ABCB1* and is activated after initial exposure to chemotherapies indicating its role in MDR. PXR activation corresponds to Pgp protein expression and is critical to the induction of Pgp expression and efflux (124-125).

Although it provides critical information, the current form of CCLF does not have much data on drugs, so we need to supplement our research with other resources. We turned to drug screening platforms and chose PRISM because of the overlap with CCLF in cell line screening. Originally, PRISM was generated from a collaboration between the Broad Institute and Sanger Institute of the United Kingdom to screen drugs across ~500 genomically characterized cell lines. PRISM cancer lines are barcoded then pooled and drugs tested via high throughput screens that measure efficacy (91).

PRISM screened 1,448 compounds against 499 cell lines. We chose PRISM over other drug screening datasets such as the Genomics of Drug Sensitivity in Cancer (GDSC) and Cancer Therapeutics Response Portal (CTRP) because PRISM had more FDA approved drugs (89-91). Since one of our goals is to optimize clinical drug selection, it was critical for our chosen dataset to incorporate FDA approved oncology drugs.

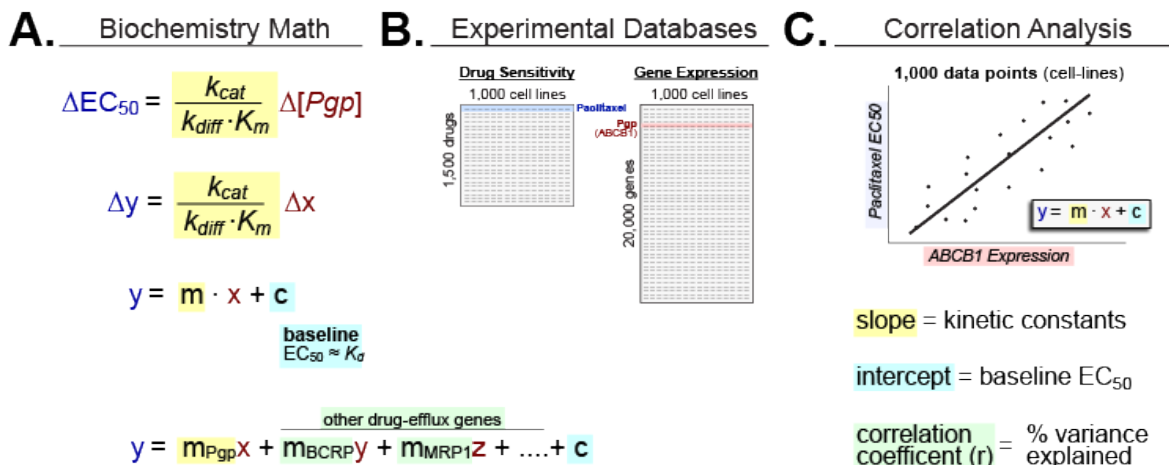


Figure 10. Mathematically Modeling MDR. The EC₅₀ shift, *ABCB1* expression and enzyme kinetics can be represented through the linear equation, $y = m \cdot x$. (A) Enzymes kinetics, $k_{cat} / (k_{diff} \cdot K_m)$, represent the slope (m) as it determines how y , the EC₅₀, changes with x , *ABCB1* expression. As a phenotype, MDR is represented by the independent contributions of several drug efflux genes. (B) CCLE has *ABCB1* mRNA expression data across 1,000 cancer cell lines. PRISM has oncology drug EC₅₀ data across 479 of 1,000 cancer cell lines. (C) A correlation analysis compares CCLE *ABCB1* mRNA expression with PRISM oncology drug EC₅₀ where single data points are individual cancer cell lines.

Combining data from CCLE and PRISM can give a functional score of MDR using strategy described in Figure 10. The Cancer Dependency Map Portal (DepMap Portal) provides a graphic use interface (<https://depmap.org/portal>,94) to perform the correlations between CCLE mRNA expression data and PRISM drug AUC data. Pearson coefficients from these CCLE and PRISM correlations offer a functional score of drug resistance. Specifically, we can use our knowledge of drug pharmacodynamics (how drugs interact with cells) and Michaelis-Menten enzyme kinetics for drug transporters to mathematically model EC₅₀ change as a linear relationship.

The assumption of first order Michaelis-Menten conditions (consistent with clinical pharmacokinetics assumptions) make the EC₅₀ proportional to Pgp expression. The enzyme substrate turnover rate (k_{cat}), enzyme-substrate affinity (K_m), and diffusion rate (k_{diff}) comprise

the slope. A higher k_{cat} means Pgp is pumping out more drug and thus increases the EC_{50} . Similarly, a lower K_m indicates greater binding affinity and increases the EC_{50} . A higher k_{diff} means that more drug is getting into the cell which would decrease the EC_{50} . As explained previously, we can approximate the EC_{50} to the K_d . For the MDR phenotype, a drug's EC_{50} is determined by multiple MDR genes of which *ABCB1* contributes. So, in a linear regression model, the slopes * expression for each drug efflux gene are additive (Figure 10A). For my research, we wanted to use *ABCB1* as a proof of concept for quantifying MDR as a multigene phenotype.

The Cancer Dependency Map Portal combines CCLE mRNA expression data with PRISM drug EC_{50} data across 479 cancer cell lines. Specifically, CCLE profiles 20,000 genes and 1,000 cancer cell lines, and PRISM encompasses 1,500 drugs across 1,000 cancer cell lines (Figure 10B). Since drug EC_{50} correlates linearly with *ABCB1* expression, the correlation coefficient (r) explains the % variance attributed to *ABCB1* expression. In our analysis, each data point is a single cancer cell line (Figure 10C). In DepMap Portal, we used the Data Explorer tool to compare *ABCB1* expression ($\log_2(TPM+)$) with individual oncology drug EC_{50} (\log_2 fold change) across 479 cancer cell lines. Under the Linear Regression section, we extracted data from the correlation including the Pearson coefficient, Spearman coefficient, Slope, Intercept and p-value for the FDA approved library of oncology drugs (94).

Figure 11A shows a general model of Michaelis-Menten enzyme kinetics for all known xenobiotic enzymes for the anthracyclines and taxanes. These xenobiotic enzymes include drug transporters and metabolism enzymes. We examined a subset of DrugBank data for the anthracyclines and taxanes (Figure 11B). We chose the anthracyclines and taxanes specifically because they are oncology drugs and frequently studied in the context of MDR. An analysis of

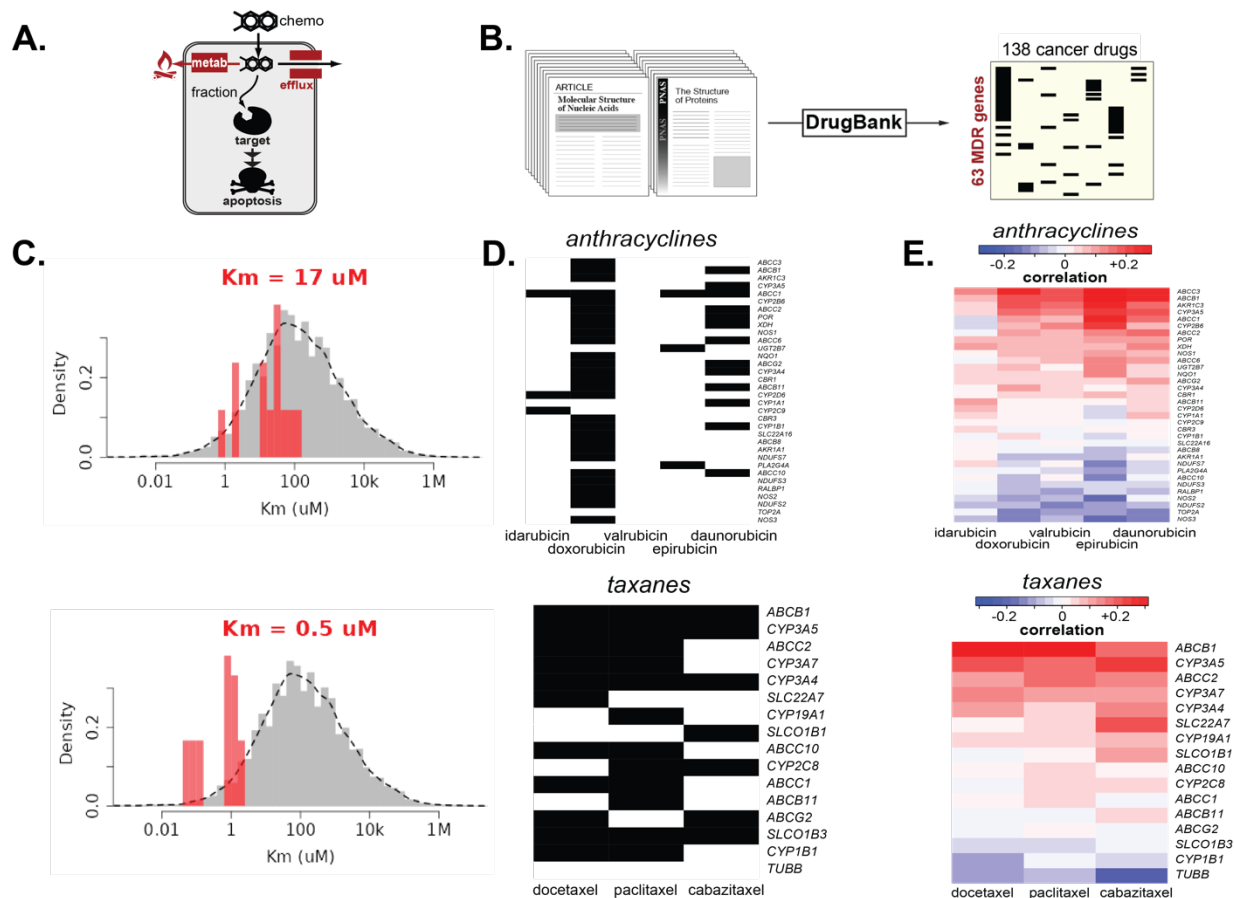


Figure 11. Correlation Analysis to Fill Gaps. Our correlation analysis fills in literature gaps and inconsistencies. (A) A fraction of drug (black) causes cytotoxicity after efflux (red) and metabolism (red). (B) DrugBank literature assigns binary definitions to Pgp substrates. (C) Literature values for K_m of Doxorubicin ($17 \mu\text{M}$) and Paclitaxel ($0.5 \mu\text{M}$) are inconsistent. (D) MDR gene-drug pairs for the anthracyclines and taxanes using DrugBank definitions. (E) MDR gene-drug pairs for the anthracyclines and taxanes using our correlation analysis.

BRENDA demonstrates no consensus K_m for the parent compounds, Doxorubicin ($17 \mu\text{M}$) or Paclitaxel ($0.5 \mu\text{M}$) (Figure 11C). For each drug class, we analyzed MDR genes focusing on ABC and Solute Carrier (SLC) drug transporters and CYP450 metabolizing enzymes with drug target genes as negative controls. The anthracyclines and taxanes have different mechanisms of action and intracellular targets. The anthracyclines target topoisomerase II and reduction-oxidation enzymes because they work through DNA disruption and reactive oxygen species accumulation. The taxanes target tubulin by interfering with microtubule depolymerization

during the cell cycle (DrugBank). A heatmap of binary DrugBank definitions (black = substrate, white = non-substrate) shows that most knowledge on the anthracyclines and taxanes is concentrated on the parent compounds, Doxorubicin and Paclitaxel (Figure 11D).

But many gaps exist in understanding most oncology drugs and MDR genes. A pilot study of our correlation analysis fills in these gaps and gives a quantitative ranking of xenobiotic enzymes with *ABCB1* at the top where a higher ranking indicates greater substrate specificity (Figure 11E). Our correlation analysis fills those gaps by bridging gene expression and drug EC_{50} through CCLE and PRISM datasets. Regenerating functional heatmaps for the same MDR genes and drugs gives a continuum of substrate specificity. For the anthracyclines and taxanes, the top three genes with the highest Pearson coefficient include *ABCB1*. Therefore, my project focuses on *ABCB1* because of its wide application in understanding MDR and oncology drugs.

To investigate the function of Pgp, we analyzed twenty oncology drugs in the FDA approved library across 479 cancer cell lines. These cell lines were chosen because they overlapped in CCLE and PRISM datasets. Both CCLE and PRISM datasets were downloaded and analyzed using the R-statistical language and new matrices created with the 479 overlapping lines for *ABCB1* and each drug. Linear regression analysis compared CCLE *ABCB1* expression with PRISM drug EC_{50} for the top twenty oncology drugs. Most drugs had a positive correlation with *ABCB1* which is consistent with Pgp as an enzyme that causes some resistance.

We expanded this analysis to all 138 oncology drugs in the FDA approved library and to other ABC genes such as *ABCC2* and *ABCG2*. Since MDR is a multigene phenotype, we expect different drugs to be resisted by different genes (Figure 12A). Each MDR gene acts like “armor” to shield the cancer cell from oncology drugs. However, each MDR “armor” is best equipped to “shield” cancer cells from a subset of drugs. Our quantitative rankings help identify which

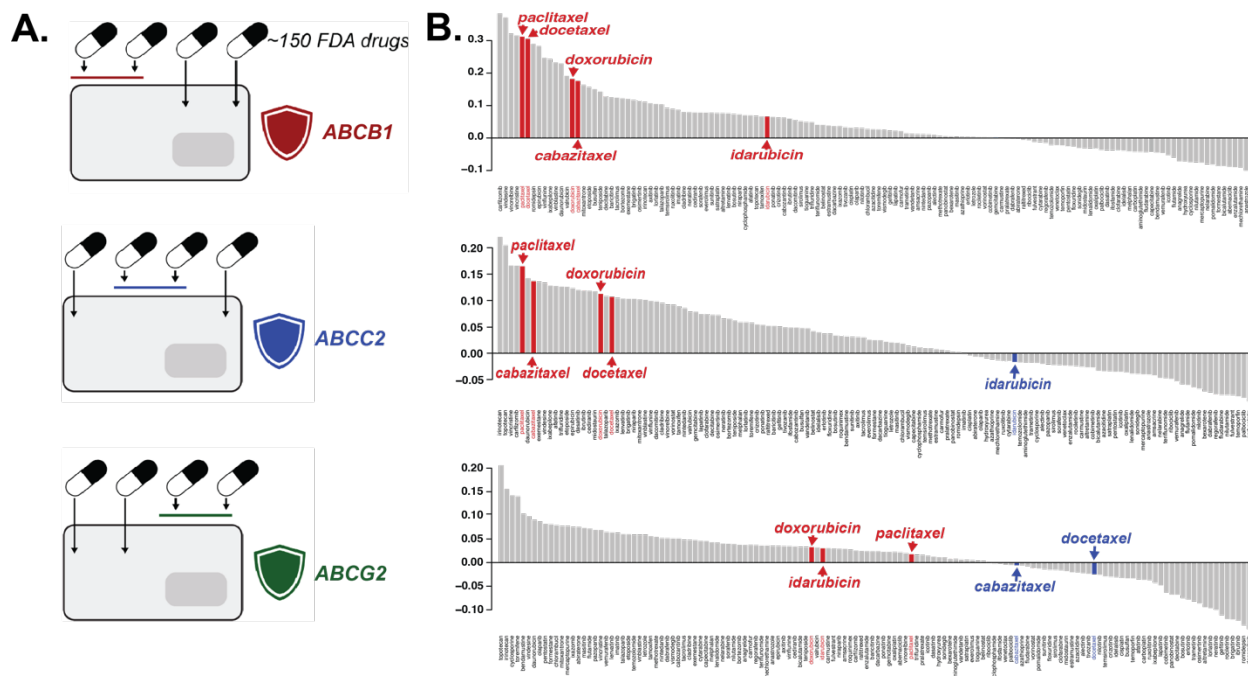


Figure 12. Quantitative Rankings of Drugs. Waterfall plots rank the FDA approved library of 138 oncology drugs by Pearson coefficient. (A) Different drugs are resisted by different “armors” such as transporters the cancer expresses to protect itself. (B) Higher (red) to lower (blue) ranked drugs are more to less likely to be resisted by the cancer where Pearson coefficients indicate the strength of MDR substrate specificity.

oncology drugs are most and least likely to pierce the MDR “armor worn” by cancer cells. Our analysis generated waterfall plots which rank 138 FDA approved oncology drugs by their Pearson coefficients which were determined from correlation analyses between ABC gene expression and drug EC_{50} across 479 cancer cell lines. Thus, the Pearson coefficient is a measure of substrate specificity for each drug-gene pair. A greater Pearson coefficient indicates greater substrate specificity and a higher probability of drug resistance.

Since our focus is on taxanes, vinca alkaloids and anthracyclines, we highlighted these drugs in the waterfall plots (Figure 12B). For *ABCB1* and *ABCC2*, most of these drugs are highly ranked except for Idarubicin which may be less of a Pgp substrate than other anthracycline drugs (126-127). Though similar, there is some variation in the rankings between *ABCB1* and *ABCC2*

which represents differences in preferred substrates for each enzyme. Many factors contribute to substrate preferences such as the drug molecular weight and chemical structure, binding affinity and enzyme binding pocket. The enzyme for *ABCG2*, Breast Cancer Resistant Protein (BCRP), is much different than Pgp which is reflected in its quantitative rankings of oncology drugs (31). *ABCG2* has a much narrower binding pocket, so drugs which are strong substrates of *ABCB1* are only moderate or weak substrates of *ABCG2*. With this analysis between gene expression and drug potency, EC_{50} is not always measurable, so we used drug area under the curve (AUC) as a surrogate which is more common (89-91). The AUC has limits which are described more in Figure 15.

Since most drugs had a positive correlation with *ABCB1* expression, we wanted to determine if quantitatively defining Pgp substrates agreed with the scientific literature. So, we used CCLE and PRISM which has Pgp expression and drug AUC data across 479 cancer lines (Figure 13C). Then, we separated 138 drugs which were listed in DrugBank and the FDA approved oncology library based on their binary definitions. Once we grouped the drugs into ‘Pgp Known’ (70 drugs) or ‘Pgp Undefined’ (68 drugs) by DrugBank definitions (85), we input their Pearson coefficients from correlations between *ABCB1* expression and drug AUC. Then, we took the average Pearson coefficient from each group and conducted a one-tailed Student’s T-test to determine if DrugBank binary definitions aligned with quantitative Pearson coefficients (Figure 13D). The T-test confirmed that Pearson coefficients correctly identified Pgp substrates in agreement with DrugBank (p-value = 0.0129). Critically, the Pgp Known drugs had a higher average Pearson coefficient than the Pgp Undefined drugs (Figure 13D).

We then ranked the FDA approved library of 138 oncology drugs in descending order by their Pearson coefficients. Since Pearson coefficients are a measure of Pgp substrate specificity, the drugs to which Pgp confers the most resistance should be the highest ranked. Our general analysis yielded >85% drugs with a positive correlation. We focused on the top ten oncology drugs which are enriched in the taxanes (Paclitaxel, Docetaxel), vinca alkaloids (Vincristine, Vinflunine, Vinblastine) and anthracyclines (Daunorubicin, Doxorubicin). The other top ten drugs were Carfilzomib, a proteasome inhibitor, Romidepsin, a histone deacetylase inhibitor and Ixabepilone, an epothilone (Figure 13D). There is some variety in the top ten drugs in class and mechanism of action supporting Pgp conferring resistance to several oncology drugs.

Our computational analysis linked *ABCB1* expression to drug AUC, but not all cell lines and drugs yielded data. In the PRISM drug screen, some drugs were not cytotoxic. Therefore, we wanted to look at EC₅₀ specifically as a quantitative metric. Additionally, we wanted to study how changes in Pgp expression changes the drug EC₅₀. Compared to our approach, Lee *et. al.* utilized two cell lines with induced Pgp expression which simplifies the study of Pgp expression on drug potency but might not accurately represent a model of acquired multidrug resistance through increased Pgp expression (126).

In this study, a high throughput screen (HTS) was conducted using compound libraries to determine cytotoxicity with differential Pgp expression (Figure 13E). These researchers used a parent KB-3-1 human cervical adenocarcinoma and Pgp overexpression subline KB-8-5-11 which they induced through incremental dosing with Colchicine (100 ng/ml) and verified through flow cytometry. For the HTS, compounds were screened against the parent line and Pgp overexpression line – and + Pgp inhibitor Tariquidar to measure the reversibility of drug resistance to compounds which were classified as Pgp drug substrates (126).

Compounds were taken from the Mechanism Interrogation Plate (MIPE) library (1,912), National Center for Advancing Translational Science pharmaceutical collection (NPC) (2,816), NCATS Pharmacologically Active Chemical Toolbox (NPACT) (5,099) and kinase inhibitor library (977). The MIPE library includes oncology compounds at preclinical, investigational and FDA approved stages. The NPC library contains compounds approved by the FDA and some drugs approved by agencies in other countries. The NPACT library has compounds with an emphasis on novel phenotypes, biological pathways and cellular processes (ncats.nih.gov/research/research-activities/compound-management).

For the HTS, cells were plated at 500 cells/well in 1536 well plates in 5 μ l of media and incubated at 37 °C and 5% CO₂ with compound for 72 hours. After 72 hours, Cell Titer-Glo reagent was added to all wells, incubated for 5 minutes and luminescence read. The drug screen yielded 90 of 10,804 compounds which were Pgp substrates and 55 of the 90 Pgp substrates which were novel. For the KB-3-1 parent line, 1,362 of the 10,804 compounds were cytotoxic. Thirty percent of the kinase, 21% of the MIPE, 10% of the NPACT and 5% of the NPC compound libraries exhibited cytotoxicity in the HTS (126).

Lee *et. al.* induced Pgp to study the effect of expression on drug EC₅₀ or [drug] required to kill 50% of cells which is a measure of cytotoxicity. The difference between dose response curves in the parent KB-3-1 and Pgp overexpression KB-8-5-11 lines is the AUC. The Δ AUC is correlated to the Δ Pgp expression and drug efflux between the cell lines. In the HTS, they gathered dose response data for the KB-3-1 parent line, KB-8-5-11 Pgp overexpression line and KB-8-5-11 line + 1 μ M Tariquidar to measure reversibility of drug resistance.

Dose response curves were plotted by the log drug (M) on the x-axis and % Activity on the y-axis. The % Activity corresponds to cell viability where -50 means 50% cell death.

Additionally, they measured the ΔAUC between the KB-3-1 parent line and KB-8-5-11 Pgp overexpression line as ΔAUC1 . The ΔAUC between the KB-8-5-11 line and + 1 μM Tariquidar is ΔAUC2 . For the 90 compounds identified as Pgp substrates, a rank order analysis was conducted which plotted ΔAUC1 against ΔAUC2 for the 90 Pgp substrates with a positive correlation ($R^2 = 0.69$) (126).

For the HTS, our lab created an online app to visualize dose response curve data in KB-3-1 and KB-8-5-11 lines for 10,804 compounds. Our online app calculates the ΔEC_{50} (fold change) in the drug-resistant vs parent lines. A greater fold change indicates stronger Pgp substrate specificity (https://douglasslab.shinyapps.io/mdr_screen/).

Since the data from Lee *et. al.* links drug ΔEC_{50} to Pgp expression, we wanted to determine if ΔEC_{50} agreed with Pgp substrates as defined by the scientific literature. So, we grouped the FDA approved oncology drug library into ‘Pgp Known’ if DrugBank classified them as Pgp substrates (70 drugs) and ‘Pgp Undefined’ if DrugBank classified them as Pgp non-substrates (68 drugs). Then, we listed the log ΔEC_{50} from Lee *et. al.* for the 138 oncology drugs and calculated the average log ΔEC_{50} for each group (Figure 13F).

We conducted a one-tailed Student’s T-test comparing DrugBank vs log ΔEC_{50} substrate definitions for each group. The T-test yielded a p-value of 0.0349 which demonstrated that log ΔEC_{50} can be used as a quantitative metric for assessing Pgp substrate specificity (Figure 13F). As with the Pearson coefficient, the Pgp Known drugs had a higher log ΔEC_{50} than the Pgp Undefined drugs. As quantitative metrics, both Pearson coefficients and log ΔEC_{50} incorporate Pgp expression which is critical for assessing MDR. Since tissues have differential expression of MDR genes, incorporating expression into quantitative metrics of substrate specificity is more accurate and predictive of drug resistance.

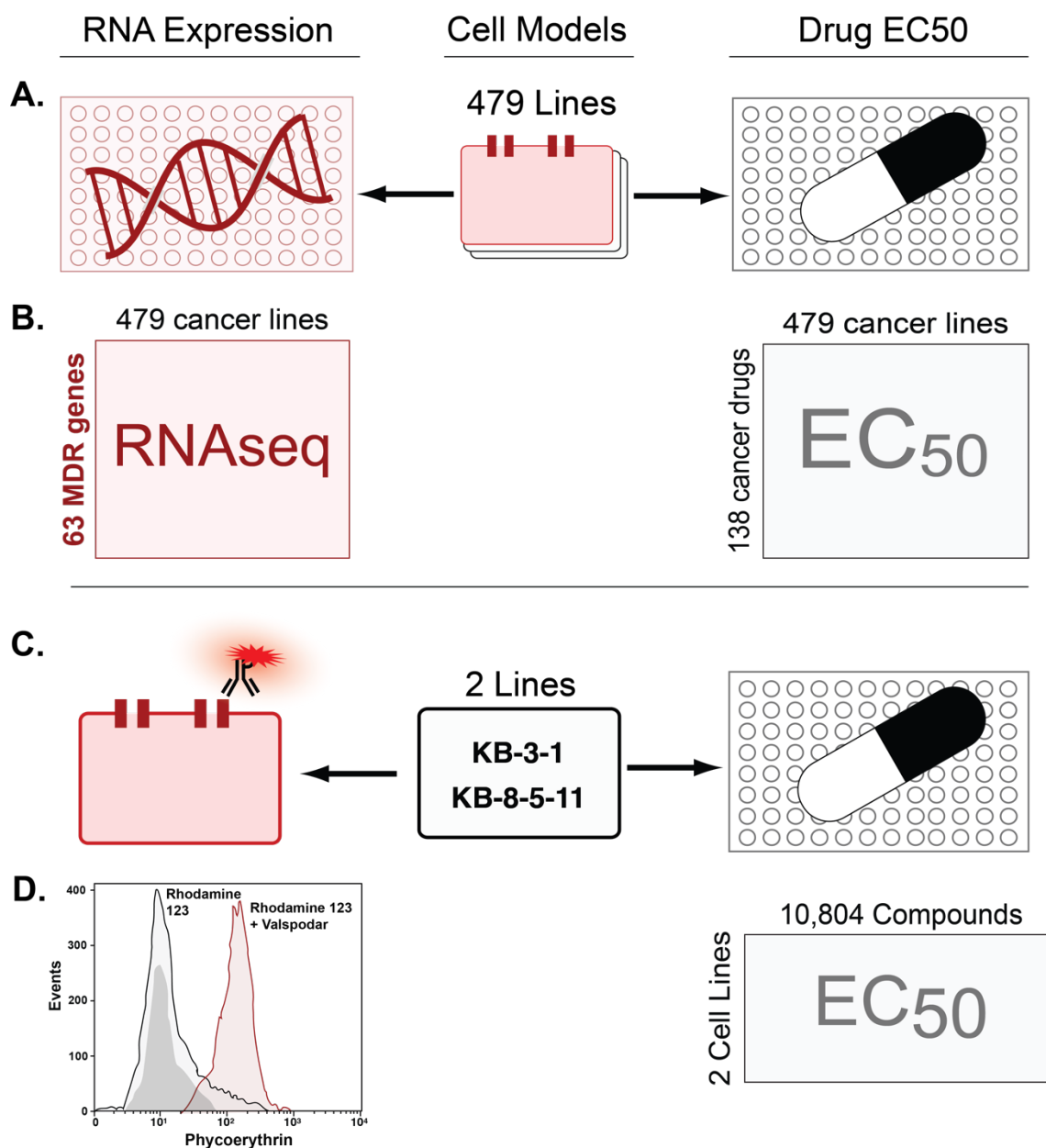


Figure 14. Approaches for Substrate Specificity Metrics. Quantitative metrics for Pgp substrate specificity are obtained through two approaches. (A) CCLE and PRISM databases characterize 479 cancer lines through mRNA expression and drug EC₅₀. (B) CCLE RNAseq analysis of 63 MDR genes and PRISM EC₅₀ analysis of 138 oncology drugs across 479 cancer lines. (C) KB-3-1 parent and KB-8-5-11 Pgp-high cancer lines characterized through protein expression and drug EC₅₀. (D) Flow cytometry analysis to quantify Pgp-mediated transport in MDR-19 cells (0.5 $\mu\text{g/ml}$ Rhodamine 123 +/- 3 $\mu\text{g/ml}$ Valspodar) with 25 μM compound identified in the drug screen of 10,804 compounds to assess Pgp substrate specificity.

Although both metrics incorporate Pgp expression, the difference is Pearson coefficients come from natural Pgp expression vs log ΔEC_{50} coming from induced Pgp expression. Additionally, Pearson coefficients were generated from an analysis of 479 cancer lines vs log ΔEC_{50} from an analysis of two cancer lines (Figure 14A and 14C). So, we then wanted to assess agreement between Pearson coefficients and log ΔEC_{50} as quantitative metrics of Pgp substrate specificity. We generated a scatter plot to study the correlation between Pearson coefficients and log ΔEC_{50} with 138 FDA approved oncology drugs (Figure 13F).

For the scatter plot, 138 drugs were plotted by their log ΔEC_{50} on the x-axis and Pearson coefficient on the y-axis. Our analysis includes a cluster of data points (drugs) with low log ΔEC_{50} and Pearson coefficients indicating these are likely weak or non-Pgp substrates. The rest of the drugs had higher log ΔEC_{50} and Pearson coefficients meaning they are likely stronger or moderate Pgp substrates. In general, there is a positive correlation between both quantitative metrics (Figure 13F). Some drugs exhibit stronger substrate specificity as measured by log ΔEC_{50} or Pearson coefficient which could be due to differences in cell lines. Lee *et. al.* used two ovarian cancer lines for their HTS vs 479 cancer lines for the PRISM screen (Figure 14A and 14C). This is evidence supporting the use of multiple quantitative metrics for the most comprehensive understanding of MDR.

Even though the PRISM screen covers more cell lines, obtaining dose response data only works when the drug is cytotoxic. If the drug is not cytotoxic, there will not be a dose response curve or EC_{50} . Once a drug enters a cell, it must bind to the intracellular target and cause cell death within the range of drug concentrations tested (Figure 15A).

Earlier, we conducted a linear regression analysis of the top twenty oncology drugs comparing CCLE *ABCB1* expression on the x-axis with drug AUC on the y-axis. We can use

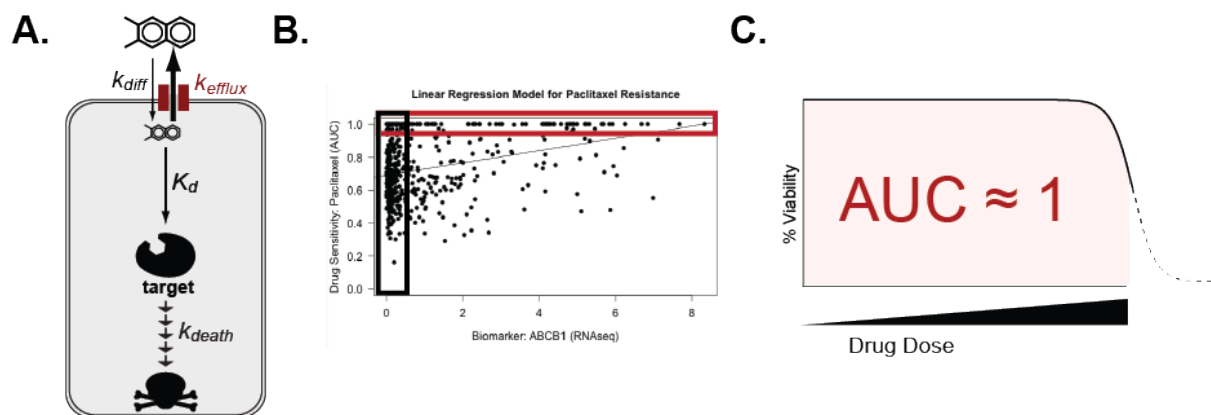


Figure 15. Limitations of AUC in Drug Screening. The AUC does not yield a measurable EC_{50} without cytotoxicity. (A) For cytotoxicity to occur, drug must bind the intracellular target and cause cell death over time. (B) In our correlation analysis, there are vertical and horizontal clusters of cell lines (single data points). The vertical cluster includes drug sensitive cell lines which have low to no *ABCB1* expression. The horizontal cluster includes drug resistant cell lines which do not exhibit cytotoxicity regardless of *ABCB1* expression. (C) An $AUC = 1$ means that the drug does not cause cytotoxicity at the drug concentrations tested or the drug is not cytotoxic to the cell line regardless of concentration.

Paclitaxel as an example of the limitations of the PRISM screen in some cell lines. In the linear regression analysis, there are vertical (black box) and horizontal (red box) clusters of cancer lines. In the vertical cluster, these cell lines have low to no *ABCB1* expression and a range of AUCs for Paclitaxel. These cell lines likely have higher drug sensitivity to Paclitaxel. In the horizontal cluster, these cell lines have low to high *ABCB1* expression and an $AUC = 1$ for Paclitaxel. Paclitaxel resistance in the low *ABCB1* expression cell lines is not due to *ABCB1* but other drug transporters or metabolizing enzymes. Paclitaxel resistance in the high *ABCB1* expression cell lines is due to *ABCB1* (Figure 15B).

As shown, AUC is a surrogate measurement of drug EC_{50} . For an $AUC = 1$, there is no dose response curve within the drug concentration range. This phenomenon can represent a few different scenarios. The first scenario is that a higher drug concentration is needed for cytotoxicity which is outside the drug screen concentrations as shown by the dotted line

extrapolation (Figure 15C). In drug screens, a standard range is typically used, and less potent drugs require a higher concentration to be cytotoxic. The second scenario is that a drug is non-toxic to the cell line regardless of concentration. This would be a likely explanation for drugs whose mechanisms of action do not cause cytotoxicity. However, we limited our analysis to oncology drugs which are cytotoxic, so the first scenario is the most plausible.

Since PRISM has potential false negatives because of dose range limitations, we investigated studies which use fluorescent probes and Pgp inhibitors to assess substrate specificity. We found a study which looked at MDR in multiple myeloma with anthracycline drugs and a Pgp modulator. Anthracyclines are oncology drugs and of great interest to us given our computational analysis classifying them as strong Pgp substrates. Thus, this paper is particularly relevant for a direct comparison with our results. Roovers *et. al.* studied a newer anthracycline, Idarubicin, in the context of multiple myeloma to see if its higher lipophilicity could increase cytotoxicity compared to Doxorubicin and Daunorubicin (127). With a higher lipophilicity, Idarubicin has the potential for better efficacy and potency in multiple myeloma treatment.

A parent multiple myeloma cell line 8226-S and two Pgp overexpression cell lines were chosen to assess cytotoxicity and uptake kinetics and Doxorubicin, Daunorubicin and Idarubicin. Pgp overexpression was induced in 8226-R7 cells with a single dose of Daunorubicin and 8226-Dox40 cells with multiple doses of Doxorubicin. This strategy is analogous to the strategy used in Lee *et. al.* to induce Pgp expression in the Pgp overexpression cancer lines (126-127).

Dose response and cytotoxicity were assessed after a 3-day incubation + drug + or - Pgp modulator, Verapamil, through the MTT colorimetric assay. The MTT assay is based on the reduction of the yellow tetrazolium salt, 3-(4,5-dimethylthiazol-2-yl)-2,5-diphenyltetrazolium

bromide (MTT), to a purple formazan crystal by live cells. Optical density (OD) was measured at 750 nm where a higher OD corresponds to more live cells (less transparent) and a lower OD indicates more cell death (more transparent). Dose response curves were plotted as drug concentration (μM) on the x-axis and OD750 on the y-axis. Data was gathered for Doxorubicin, Daunorubicin and Idarubicin across the three cell lines (127).

The 8226-S parent line exhibited the greatest cytotoxicity with Idarubicin having the most potency and Doxorubicin having the least potency. The 8226-R7 Pgp overexpression line demonstrated more resistance to all three drugs, decreasing their potency (127). Idarubicin still had the best potency and Doxorubicin the least potency. Lastly, the 8226-Dox40 Pgp overexpression line had even more resistance to all three drugs, with no drug achieving 100% cell death at the highest drug concentration (4 μM) (127). However, Idarubicin still had the greatest potency of the three drugs. Since drug potency decreased with increasing Pgp expression, it follows that Idarubicin could be a weak Pgp substrate. The ΔEC_{50} for Idarubicin was much less than for Doxorubicin and Daunorubicin across the three cell lines (127-128).

The same experiment was conducted with the addition of 50 μM Verapamil, a first generation Pgp inhibitor. In theory, the stronger Pgp substrates, Doxorubicin and Daunorubicin, will exhibit more potency with Verapamil in the Pgp overexpression cell lines. As expected, the addition of Verapamil did not significantly change the dose response curves in the 8226-S parent line. In the 8226-R7 line, Doxorubicin and Daunorubicin were slightly more potent than without Verapamil. In the 8226-Dox40 line, the difference was more pronounced where the addition of Verapamil achieved 100% cell death with Doxorubicin, Daunorubicin and Idarubicin at 2 μM and 4 μM of drug (127). These results emphasize optimal drug selection for cancer treatment. Pgp inhibitors such as Verapamil are best used in Pgp-high cell lines, and drugs which are

resisted by Pgp need to be given in cancers with low or no Pgp for optimal clinical results.

To measure Pgp expression, Roovers *et. al.* used the anthracyclines as fluorescent probes and flow cytometry across 8226-S, 8226-R7 and 8226-Dox40 lines (Figure 16A). Essentially, the anthracyclines' fluorescence is an indirect measure of drug accumulation inside cells. As Pgp expression increases, more anthracycline can be pumped out and the fluorescence decreases. So, the $\Delta[E]$ is directly proportional to the $\Delta[\text{Probe}]$ (Figure 16A).

They used flow cytometry to quantify Pgp protein expression across all three multiple myeloma cell lines (Figure 16C left). For this analysis, 4×10^5 cells were incubated with 10 μl of 50 $\mu\text{g}/\text{ml}$ mouse Pgp monoclonal antibody MRK16 for 60 minutes at room temperature. Cells were then washed with a phosphate buffered saline-fetal calf serum (PBS-FCS) buffer and incubated for 15 minutes at room temperature with 0.5 μg of goat anti-mouse IgG2a-FITC.

Results confirmed the highest Pgp expression in 8226-Dox40 cells followed by slightly less expression in 8226-R7 cells and basal expression in the 8226-S cells (127). Since flow cytometry measures Pgp expression, it confirms the quantity of Pgp protein at the cell surface but does not assess functionality of the enzyme as a drug transporter (Figure 16C left).

To determine Pgp functionality, Rhodamine123 was used as a fluorescent probe to measure efflux. Rhodamine123 is a cell permeable, green, fluorescent dye that is also a known Pgp substrate. In these studies, the Rhodamine123 efflux ratio (Rho123 fluorescence – Verapamil / Rho123 fluorescence + Verapamil) was determined where a smaller efflux ratio indicates greater Pgp functionality (Figure 16B left). The cells were washed, resuspended in culture medium at 8×10^5 cells/ml with 125 nM Rho123 and incubated at 37 °C for 10 minutes. The cells were washed twice, resuspended in culture medium and plated in 24 well plates at 0.5 ml/well. After a 20-minute CO₂ incubation, the cells were pelleted, washed and resuspended

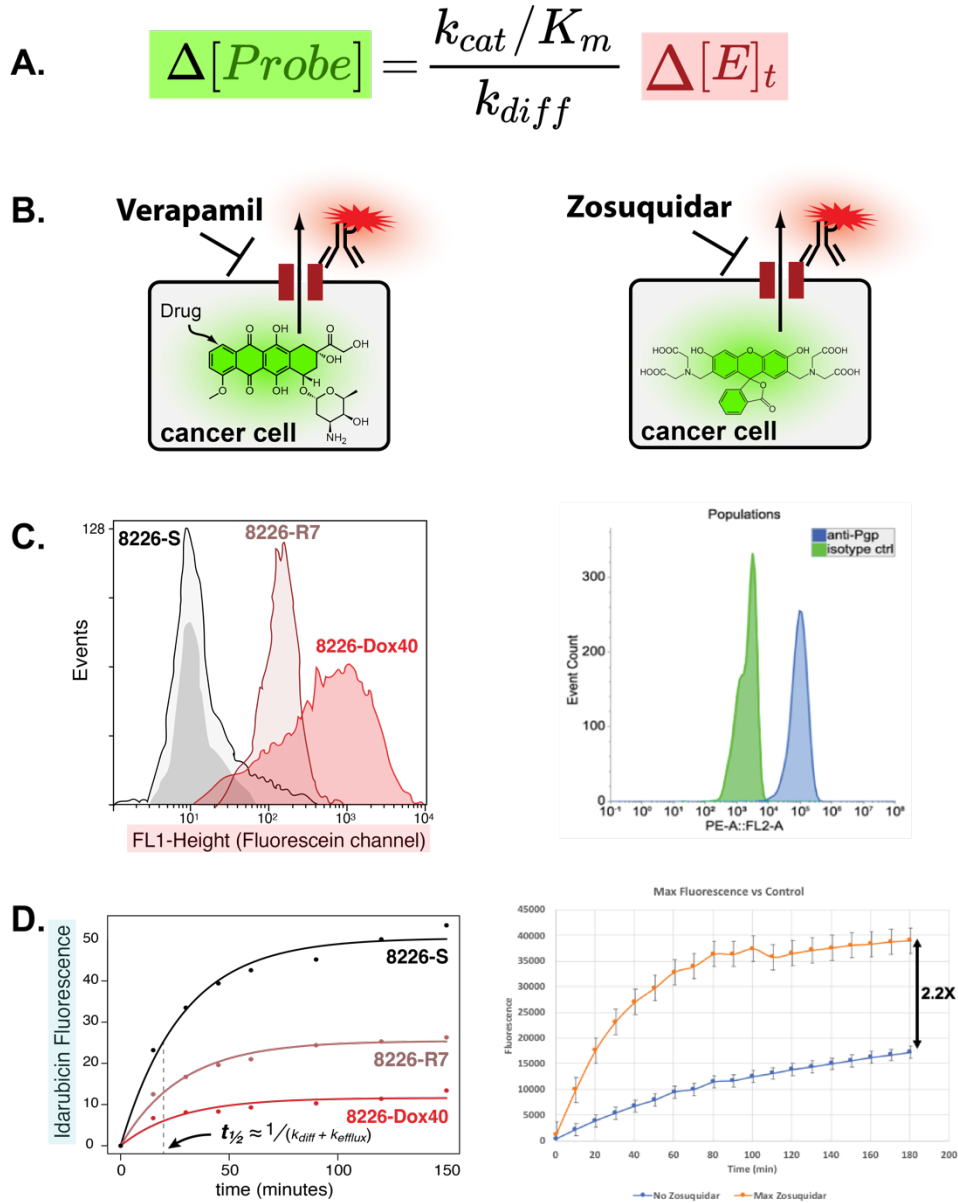


Figure 16. Fluorescent Probes for Drug Screening. (A) Probe fluorescence inversely changes with MDR expression where lower fluorescence indicates higher expression. (B) Pgp substrate specificity is measured through intracellular accumulation of drug (Roovers *et. al.*) or fluorescent dye (Ashley) +/- addition of Pgp inhibitor. (C) Flow cytometry quantifies Pgp expression in multiple myeloma (Roovers *et. al.*) or breast cancer (Ashley) cell lines through antibody staining. (D) Fluorescent microscopy tracks uptake of Idarubicin (Roovers *et. al.*) or Zosuquidar (Ashley) into cells over time. The kinetics of uptake are modeled through k_{diff} and k_{efflux} .

in 500 μ l of PBS-FCS and run through flow cytometry (127). Using 8226-S cells as a control (efflux ratio = 1), the Pgp overexpression lines had lower efflux ratios (30% in 8226-R7, 10% in 8226-Dox40) which corresponded with Pgp function (Figure 16B left).

Given its higher lipophilicity and better potency, uptake kinetics were measured for Daunorubicin and Idarubicin (Figure 16D left). Chemically, Daunorubicin is more similar in structure to Idarubicin than Doxorubicin, so Daunorubicin was included for comparison. In this experiment, 1 μ M of anthracycline was added to 8226-S, 8226-R7 and 8226-Dox40 cells and drug uptake monitored with fluorescent microscopy. Drug uptake measurements were taken periodically over 120 minutes. Data was plotted as time (minutes) on the x-axis vs mean fluorescence intensity (MFI) on the y-axis (127). After 60 minutes, the MFI had peaked in the three cell lines indicating the maximum rate of drug uptake (Figure 16D left).

This curve can be used to calculate the $t_{1/2}$ or time taken for half-maximal drug accumulation. Since the $t_{1/2}$ is determined by both diffusion and efflux, it can be represented as $1 / (k_{diff} + k_{efflux})$ where greater rates indicate less time for maximum accumulation of drug. However, if little to no drug is accumulated as with Pgp-high cells, the maximum fluorescence will be relatively low. As expected, the 8226-S parent line had the greatest fluorescence indicating the most intracellular accumulation. The 8226-R7 cells had the next greatest fluorescence followed by the 8226-Dox40 cells (Figure 16D left). Relative to Daunorubicin, Idarubicin accumulation occurred seven times faster which could be attributed to Idarubicin's higher lipophilicity (127).

Subsection 3: Experimental Work to Quantify MDR

Roovers *et al.* studied intracellular concentration and MDR simultaneously because the anthracyclines are naturally fluorescent Pgp substrates (Figure 16B left). But the MTT assay

does not work for non-toxic compounds, and most oncology drugs are not naturally fluorescent. So, we wanted to develop a competitive assay with a known fluorophore and Pgp substrate to estimate intracellular concentrations of drug for non-toxic and non-fluorescent compounds (Figure 16A).

With the AUC limitation of PRISM, we chose Calcein acetomethylester (AM) as a fluorescent probe to assess Pgp substrate specificity *in-vitro* (Figure 17). Calcein AM is a known Pgp substrate, cell permeable, fluorescent green dye (129). Calcein AM easily diffuses into cells where the AM is cleaved by esterase enzymes in live cells. Once the AM is cleaved, Calcein fluoresces green inside cells. Without the acetomethylester component, Calcein cannot leave the cell without being pumped out by Pgp (129).

For our work, we chose DU4475 as a Pgp-high cancer line. DU4475 is a ductal adenocarcinoma with the highest Pgp expression of 71 breast cancer lines and fourth highest Pgp expression of 1,000 cancer lines. DU4475 was used as our cell line model because of its high *ABCB1* expression and low expression of other ABC genes including *ABCC1* and *ABCG2* which could be confounding variables (depmap.org/portal/,94).

We chose drugs for the screen based on Pgp substrate specificity rankings from their Pearson coefficients, so the screen included 76 strong, moderate, weak and non-Pgp substrates. The premise of the screen is a competitive binding assay where Calcein competes with drug for binding to Pgp (Figure 17C, Figure 18A). The intracellular accumulation of Calcein and resulting fluorescence is a measure of Pgp substrate specificity. The higher fluorescence will be achieved with drugs that are stronger Pgp substrates as they will outcompete Calcein for binding to Pgp (Figure 18A). We began this work with fluorescent microscopy (Figure 17A) to optimize

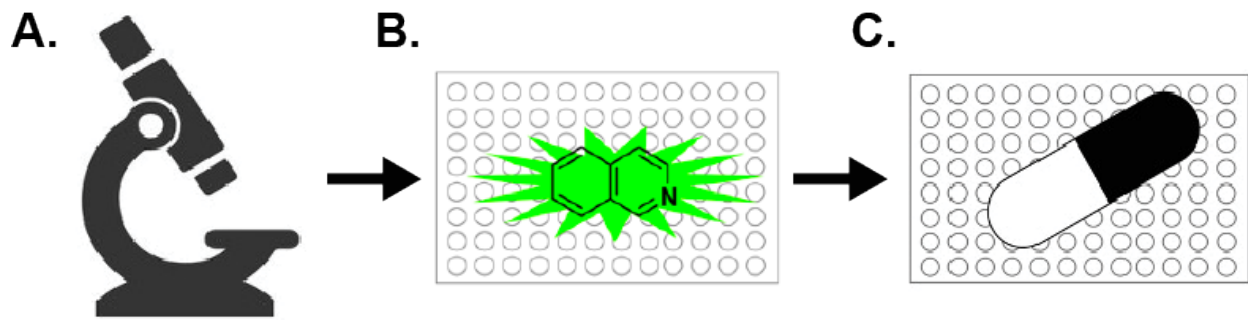


Figure 17. Experimental Pipeline for Assay Development. (A) Fluorescent microscopy to optimize cell culture and Calcein AM concentration. (B) Plate-based assay with Calcein AM to optimize competition with Pgp inhibitors. (C) Plate-based screen with Calcein AM to test 76 drugs from the FDA approved oncology drug library.

cell culture conditions and Calcein concentration, then transitioned to a 96 well plate assay (Figure 17B) and converted it into a drug screen (Figure 17C).

For the assay, first to third generation Pgp inhibitors were used as positive controls for Calcein accumulation and fluorescence. These included first generation Pgp inhibitors Cyclosporine, Nicardipine and Verapamil and third generation Pgp inhibitors Dofequidar, Elacridar, Encequidar, ONT-093, PGP-4008, Tariquidar and Zosuquidar (Figure 18B). For both the inhibitor and drug screens, DU4475 cells were trypsinized, incubated at 37 °C and 5% CO₂ for 5 minutes, resuspended in sterile PBS and counted with a hemocytometer and trypan blue (Appendix A, Protocol 1).

For the competitive binding assay, 100,000 cells/well were used and 100 µl of cells/PBS plated in a 96 well plate (Figure 18A). We tested ten Pgp inhibitor concentrations from 5 µM to 0.5 pM (Figure 18B) and added 100 µl of each inhibitor concentration to the 96 well plate. Then, 100 µl of a 1% DMSO in PBS solution was added to a subset of wells in the 96 well plate to serve as negative controls. Lastly, a staining solution was prepared of 0.36 µM Calcein AM in sterile PBS and 100 µl added to all wells in the 96 well plate. After addition, the fluorescence

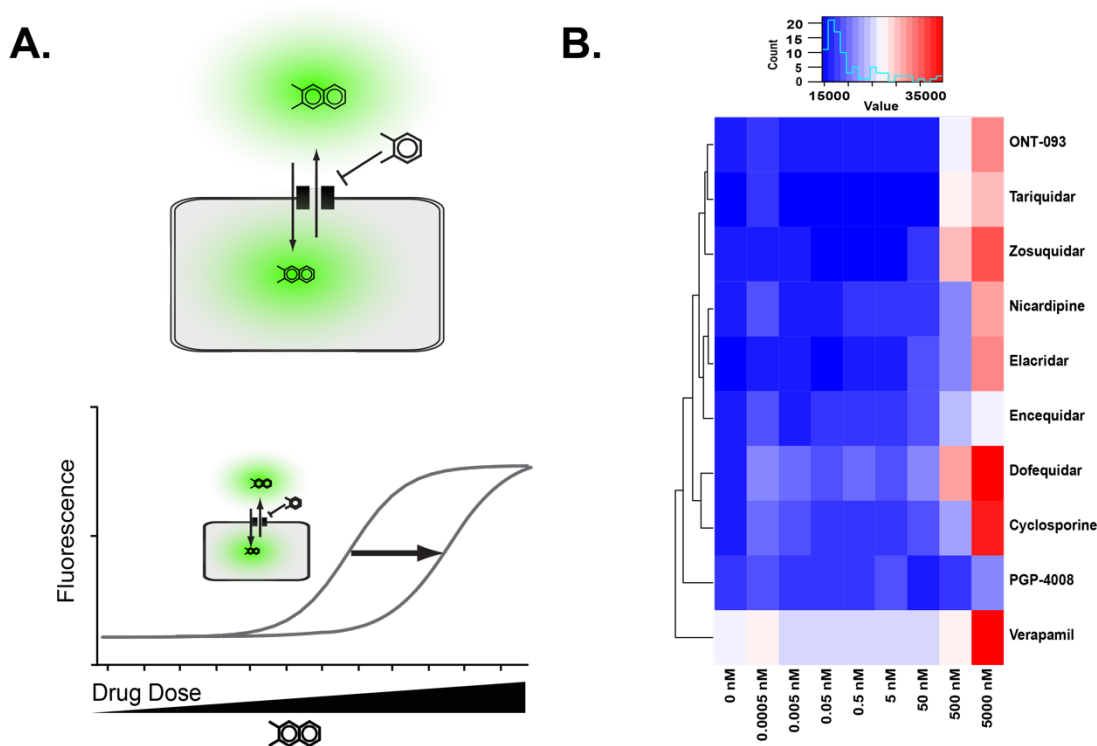


Figure 18. Drug Screen Measures Potency. Our Calcein AM plate-based screen measures drug potency. (A) The assay works by measuring substrate specificity through Pgp competitive binding between Calcein and drug. Potency is assessed by the drug dose at which fluorescence (Calcein intracellular accumulation) is half-maximal. (B) Our drug screen measured fluorescence dose response for ten first and third generation Pgp inhibitors from 0.0005 to 5000 nM.

(Calcein AM excitation = 485 nm, emission = 526 nm) was measured every 10 minutes for 6 hours at 5% CO₂ and 37 °C (Appendix A, Protocol 1). Results showed that the best signal to noise was achieved with 5 μM Pgp inhibitor. As expected in a Pgp-high line, the third generation Pgp inhibitors demonstrated the best efficacy measured as maximum fluorescence with Dofequidar demonstrating the best potency (Figure 18B).

For the drug screen, 100,000 cells/well were used and 100 μl of cells/PBS plated in a 96 well plate (Figure 19A). As before, 100 μl of a 1% DMSO in PBS solution was added to a subset of wells in the 96 well plate to serve as negative controls. Thirty μl of each drug and 70 μl of

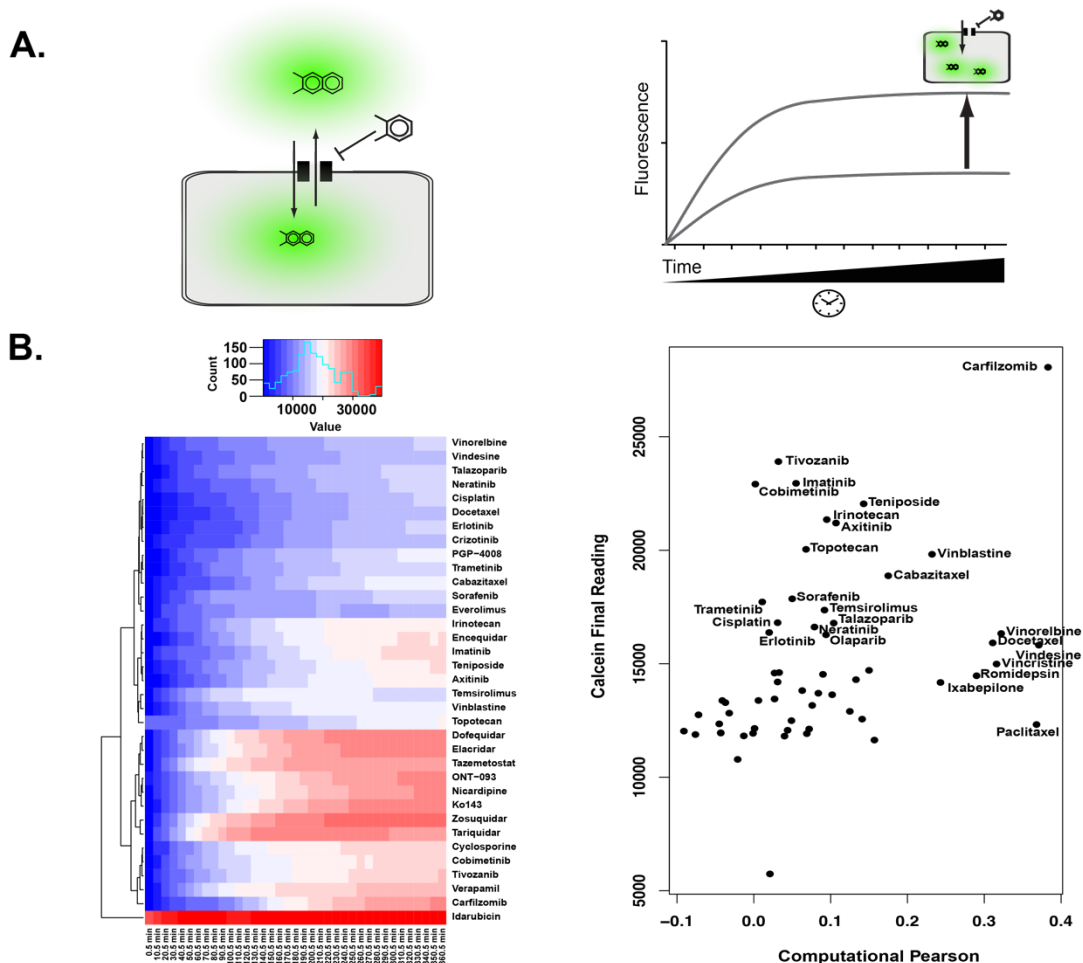


Figure 19. Drug Screen Measures Efficacy. Our Calcein AM plate-based screen measures drug efficacy. (A) The assay works by measuring substrate specificity through Pgp competitive binding between Calcein and drug. Efficacy is assessed by the maximum fluorescence (Calcein intracellular accumulation, 100% competition). (B) Our drug screen measured fluorescence for 76 oncology drugs across 360.5 min with readings taken every 10 min. Cells were incubated at 37 °C and 5% CO₂ for the drug screen. Pearson coefficients positively correlate with drug efficacy from the Calcein assay, especially for strong Pgp substrates.

PBS were added to each well in the 96 well plate (Figure 19B). Lastly, a staining solution was prepared of 0.36 μM Calcein AM in sterile PBS and 100 μl added to all wells in the 96 well plate. After addition, the fluorescence (Calcein AM excitation = 485 nm, emission = 526 nm) was measured every 10 minutes for 6 hours at 5% CO₂ and 37 °C (Appendix A, Protocol 2).

Results identified many top Pgp substrates in agreement with our correlation analysis such as Carfilzomib and Vinblastine. It also identified some kinase inhibitors such as Cobimetinib and Tivozanib as Pgp substrates (Figure 19B).

Using beads and ~10,000 single cells, flow cytometry analysis quantified ~50,000 Pgp per cell in the DU4475 line (Appendix A, Protocol 3). Briefly, DU4475 cells were centrifuged, counted with a hemocytometer and trypan blue then diluted to 1 million/ml. DU4475 cells were washed in MACS buffer (500 ml pH 7.4 PBS, 0.5 mM EDTA, 1% BSA) and resuspended in MACS buffer at 1 million/ml. Then, 4 μ l of block was added for 3 μ M IgG antibody and incubated for 5 minutes at room temperature. A 3x, 10x, 30x and 100x dilution of IgG antibody was added to Pgp-specific phycoerythrin antibody and incubated on ice for 30 minutes. Then, the samples were run through a flow cytometer to stain the cells for Pgp (Appendix A, Protocol 3). Results of Pgp isotype control and Pgp-stained with phycoerythrin antibody indicates two distinct populations which verify a much higher expression of Pgp in DU4475 cells (Figure 16C right).

To measure Calcein AM uptake, 100,000 cells/well DU4475 cells were plated in a 96 well plate with 1 μ M Calcein AM + and - 5 μ M of Pgp inhibitor Zosuquidar. After addition, fluorescence (Calcein AM excitation = 485 nm, emission = 526 nm) was measured every 10 minutes for 3 hours at 5% CO₂ and 37 °C (Appendix A, Protocol 4). Data was plotted as time (minutes) on the x-axis vs fluorescence on the y-axis (Figure 16B right). For this assay, Zosuquidar was chosen as a selective Pgp inhibitor because it has been well characterized in the scientific literature. At endpoint, there was a 2.2X difference in Calcein uptake within DU4475 cells based on fluorescence + and - Zosuquidar. Additionally, this analysis measures the time needed for uptake to occur which was ~60 minutes for DU4475 cells + Zosuquidar (Figure 16D

right). This analysis mirrors Roovers *et. al.* data for the 8226-S and 8226-Dox40 cell lines where the higher fluorescence in the 8226-S parent line indicates lower rates of diffusion and efflux from less Pgp expression. In our study, the higher fluorescence in the + Zosuquidar group indicates lower rates of diffusion and efflux from selective Pgp inhibition.

Lee *et. al.* and our analysis both used quantitative metrics (log EC₅₀ shift or Pearson coefficient) to assess Pgp substrate specificity (Figure 13F). Both quantitative metrics statistically agree with DrugBank binary definitions of Pgp substrates (Figure 13D and 13F). Additionally, the measurability of these quantitative metrics is dependent on cytotoxicity.

In contrast, Lee *et. al.* induced Pgp expression vs our use of cancer lines with natural Pgp expression. Lee *et. al.* used two cell lines (Figure 14C) whereas we used a combination of databases which covered 479 cell lines (Figure 14A). Lee *et. al.* investigated oncology and non-oncology drugs in their 10,804-compound screen (Figure 14D). We focused exclusively on oncology drugs in our 76-drug screening assay (Figure 19B).

Natural Pgp expression more accurately reflects actual cellular physiology with multiple drug transporters. But for studying Pgp, two cell lines is easier to manage and directly compare Pgp expression. For assessing MDR more generally, 479 cell lines offers a more comprehensive analysis and is widely applicable to multiple cancers. For the drug screen, including non-oncology drugs allowed for the identification of novel Pgp substrates which is critical to extending our understanding of Pgp as a drug pump.

Roovers *et. al.* and our analysis used flow cytometry to quantify Pgp expression in the cell lines using antibody (Figure 16C). Additionally, both studies used Pgp inhibitors to assess the functionality of Pgp protein at the cell membrane surface (Figure 16B). Both measured uptake kinetics of fluorescent drug or Calcein as fluorescent probes over time (Figure 16D).

In contrast, Roovers *et. al.* induced Pgp expression vs our analysis which used a cell line with naturally high Pgp expression. Although both studies used Pgp inhibitors, Roovers *et. al.* used the first generation Pgp modulator, Verapamil, and we used a third generation selective Pgp inhibitor, Zosuquidar (Figure 16B). Roovers *et. al.* obtained three cell lines of various Pgp expression to study efflux. Alternatively, we used one cell line of high Pgp expression (Figure 16D). Since their work focused on the anthracyclines, Roovers *et. al.* could use these drugs as fluorescent probes. Most of our work includes non-fluorescent drugs, so we used Calcein AM as a surrogate fluorescent probe.

Natural Pgp expression more accurately reflects cellular physiology but could introduce complexities for studying Pgp. As a selective Pgp inhibitor, Zosuquidar is better for assessing Pgp specifically whereas Verapamil is better for assessing MDR from multiple drug pumps as a Pgp modulator. Having three cell lines of incrementally higher Pgp expression is better correlated to dose response curves than a single cell line. Lastly, using drug as a fluorescent probe is simpler, but Calcein AM allows for the study of non-fluorescent drugs which comprise most of the FDA approved library.

To conclude, we can revisit the metrics presented in this work by reconciling computational and experimental definitions to more comprehensively define MDR. As a database, DrugBank is naturally tailored to clinicians with information but has expanded to include more data on pharmacokinetics and enzyme substrate specificity (85). Unfortunately, due to its reliance on the scientific literature, DrugBank is limited to binary definitions of MDR substrates to create a consistent metric across experimental platforms.

CCLE offers mRNA expression data on ~1,000 cancer lines. PRISM offers drug screening data on 479 of the CCLE cancer lines through the DepMap Portal web interface (90-

91). Combining CCLE and PRISM data offers a linear correlation between gene expression and drug AUC within the context of MDR. This linear correlation yields Pearson coefficients which are a quantitative metric of enzyme substrate specificity. Pearson coefficients enable continuous drug classification where larger coefficients indicate stronger substrate specificity for MDR enzymes.

As a cancer phenotype, MDR depends on multiple factors including gene expression, enzyme kinetics and diffusion. For each cell and tissue, these factors have wide variability due to natural physiological roles, cellular phenotypes and function. These databases help reconcile these differences and contribute to a more complete picture of MDR in general. Bridging gene expression with enzyme kinetics is critical to redefining MDR quantitatively for optimizing drug selection in the clinic.

Prior scientific literature provided the foundation for EC_{50} (potency) and fluorescence (efficacy) as experimental metrics for assessing MDR substrate specificity. A combination of *in-vitro* approaches including flow cytometry, fluorescent microscopy and drug screens is necessary for studying Pgp substrate specificity. Pgp substrate specificity cannot be quantified by a single metric, but our analysis incorporates diffusion and enzyme kinetics into our EC_{50} experimental metric. By taking drug EC_{50} and dividing it by gene expression, we can standardize drug EC_{50} to any tissue or cancer.

The current research provides the foundation for measuring MDR quantitatively as a proof-of-concept through Pgp. In the future, this work can be expanded to elucidate the quantitative contributions of other non-*ABCB1* ABC genes to the MDR phenotype in cancer.

REFERENCES

1. Zahreddine, H. *et. al.* Mechanisms and Insights into Drug Resistance in Cancer. *Frontiers in Pharmacology*. 2013, 4:1-8.
2. Burchenal, J.H. *et. al.* Studies on the Mechanisms of Action of Various Phthalimide Derivatives by Cross-Resistance and Tissue Culture. *Cancer Research*. 1963, 23:1364-1374.
3. Hagmark, A. Studies on Resistance against 5-Fluorouracil: II. Thymidylate Synthetase from Drug-Resistant Tumor Lines. *Cancer Research*. 1962, 22:568-572.
4. Harrap, K.R. *et. al.* The Selectivity of Action of Alkylating Agents and Drug Resistance. II. A Comparison of the Effects of Alkylating Drugs on Growth Inhibition and Cell Size in Sensitive and Resistant Strains of the Yoshida Ascites Sarcoma. *British Journal of Cancer*. 1969, 23:227-234.
5. Kessel, D. *et. al.* Uptake and Retention of Daunomycin by Mouse Leukemic Cells as Factors in Drug Response. *Cancer Research*. 1968, 28:938-941.
6. Biedler, J.L. *et. al.* Cellular Resistance to Actinomycin D in Chinese Hamster Cells *in Vitro*: Cross-Resistance, Radioautographic, and Cytogenetic Studies. *Cancer Research*. 1970, 30:1174-1184.
7. Danø, K. Active Outward Transport of Daunomycin in Resistant Ehrlich Ascites Tumor Cells. *Biochimica et Biophysica Acta*. 1973, 323:466-483.
8. Ling, V. *et. al.* Reduced Permeability in CHO Cells as a Mechanism of Resistance to Colchicine. *Journal of Cellular Physiology*. 1974, 83:103-116.

9. Carlsen, S.A. *et. al.* Modulation of Membrane Drug Permeability in Chinese Hamster Ovary Cells. *Biochimica et Biophysica Acta*. 1976, 455:900-912.
10. Juliano, R.L. *et. al.* A Surface Glycoprotein Modulating Drug Permeability in Chinese Hamster Ovary Cell Mutants. *Biochimica et Biophysica Acta*. 1976, 455:152-162.
11. Riordan, J.R. *et. al.* Purification of P-glycoprotein from Plasma Membrane Vesicles of Chinese Hamster Ovary Cell Mutants with Reduced Colchicine Permeability. *Journal of Biological Chemistry*. 1979, 254:12701-12705.
12. Ling, V. *et. al.* Dominance of Colchicine Resistance in Hybrid CHO Cells. *Somatic Cell Genetics*. 1978, 4:193-200.
13. Dalton, W.S. *et. al.* Characterization of a New Drug-Resistant Human Myeloma Cell Line That Expresses P-Glycoprotein. *Cancer Research*. 1986, 46:5125-5130.
14. Dalton, W.S. *et. al.* Immunohistochemical Detection and Quantitation of P-Glycoprotein in Multiple Drug-Resistant Human Myeloma Cells: Association with Level of Drug Resistance and Drug Accumulation. *Blood*. 1989, 73:747-752.
15. Keizer, H.G. *et. al.* Correlation of Multidrug Resistance with Decreased Drug Accumulation, Altered Subcellular Drug Distribution, and Increased P-Glycoprotein Expression in Cultured SW-1573 Human Lung Tumor Cells. *Cancer Research*. 1989, 49:2988-2993.
16. Shen, D.W. *et. al.* Human Multidrug-Resistant Cell Lines: Increased *mdr1* Expression Can Precede Gene Amplification. *Science*. 1986, 232:43-45.
17. Cole, S.P. *et. al.* Overexpression of a Transporter Gene in a Multidrug-Resistant Human Lung Cancer Cell Line. *Science*. 1992, 258:1650-1654.

18. Cole, S.P.C. Targeting Multidrug Resistance Protein 1 (MRP1, ABCC1): Past, Present, and Future. *Annual Review of Pharmacology and Toxicology*. 2014, 54:95-117.
19. Doyle, L.A. *et al.* A Multidrug Resistance Transporter from Human MCF-7 Breast Cancer Cells. *Biological Sciences*. 1998, 95:15665-15670.
20. Allikmets, R. *et al.* A Human Placenta-Specific ATP-Binding Cassette Gene (ABCP) on Chromosome 4q22 that is Involved in Multidrug Resistance. *Cancer Research*. 1998, 58:5337-5339.
21. Miyake, K. *et al.* Molecular Cloning of cDNAs which are Highly Overexpressed in Mitoxantrone-Resistant Cells. *Cancer Research*. 1999, 59:8-13.
22. Mao, Q. *et al.* Role of the Breast Cancer Resistance Protein (BCRP/ABCG2) in Drug Transport—an Update. *AAPS Journal*. 2015, 17:65-82.
23. Aller, S.G. *et al.* Structure of P-Glycoprotein Reveals a Molecular Basis for Poly-Specific Drug Binding. *Science*. 2009, 323:1718-1722.
24. Jin, M.S. *et al.* Crystal Structure of the Multidrug Transporter P-glycoprotein from *Caenorhabditis elegans*. *Nature*. 2012, 490:566-569.
25. Li, J. *et al.* Refined Structures of Mouse P-glycoprotein. *Protein Science*. 2014, 23:34-46.
26. Szewczyk, P. *et al.* Snapshots of Ligand Entry, Malleable Binding and Induced Helical Movement in P-glycoprotein. *Acta Crystallographica Section D*. 2015, 71:732-741.
27. Ward, A.B. *et al.* Structures of P-glycoprotein Reveal its Conformational Flexibility and an Epitope on the Nucleotide-Binding Domain. *Proceedings of the National Academy of Sciences*. 2013, 110:13386-13391.

28. Johnson, Z.L. *et al.* Structural Basis of Substrate Recognition by the Multidrug Resistance Protein MRP1. *Cell*. 2017, 168:1075-1085.
29. Rosenberg, M.F. *et al.* The Human Breast Cancer Resistance Protein (BCRP/ABCG2) Shows Conformational Changes with Mitoxantrone. *Structure*. 2010, 18:482-493.
30. Gottesman, M.M. *et al.* Overview: ABC Transporters and Human Disease. *Journal of Bioenergetics and Biomembranes*. 2001, 33:453-458.
31. Robey, R.W. *et al.* Revisiting the Role of Efflux Pumps in Multidrug-Resistant Cancer. *Nature Reviews Cancer*. 2018, 18:452-464.
32. van Helvoort, A. *et al.* MDR1 P-Glycoprotein is a Lipid Translocase of Broad Specificity, while MDR3 P-Glycoprotein Specifically Translocates Phosphatidylcholine. *Cell*. 1996, 87:507-517.
33. Ueda, K. *et al.* Human P-glycoprotein Transports Cortisol, Aldosterone, and Dexamethasone, but not Progesterone. *Journal of Biological Chemistry*. 1992, 267:24248-24252.
34. Lam, P. *et al.* Bile Acid Transport in Sister of P-Glycoprotein (ABCB11) Knockout Mice. *Biochemistry*. 2005, 44:12598-12605.
35. Jedlitschky, G. *et al.* ATP-Dependent Transport of Glutathione S-Conjugates by the Multidrug Resistance-Associated Protein. *Cancer Research*. 1994, 54:4833-4836.
36. Leier, I. *et al.* The MRP Gene Encodes an ATP-Dependent Export Pump for Leukotriene C4 and Structurally Related Conjugates. *Journal of Biological Chemistry*. 1994, 269:27807-27810.
37. Jedlitschky, G. *et al.* Transport of Glutathione, Glucuronate, and Sulfate Conjugates by the MRP Gene-Encoded Conjugate Export Pump. *Cancer Research*. 1996, 56:988-994.

38. Jedlitschky, G. *et. al.* ATP-Dependent Transport of Bilirubin Glucuronides by the Multidrug Resistance Protein MRP1 and its Hepatocyte Canalicular Isoform MRP2. *Journal of Biochemical and Molecular Toxicology*. 1997, 327:305-310.
39. Zhang, S. *et. al.* Flavonoids Are Inhibitors of Breast Cancer Resistance Protein (ABCG2)-Mediated Transport. *Molecular Pharmacology*. 2004, 65:1208-1216.
40. Suzuki, M. *et. al.* ABCG2 Transports Sulfated Conjugates of Steroids and Xenobiotics. *Journal of Biological Chemistry*. 2003, 278:22644-22649.
41. Litman, T. *et. al.* Competitive, Non-Competitive and Cooperative Interactions between Substrates of P-glycoprotein as Measured by its ATPase Activity. *Biochimica et Biophysica Acta*. 1997, 1361:169-176.
42. Garrigos, M. *et. al.* Competitive and Non-Competitive Inhibition of the Multidrug-Resistance-Associated P-glycoprotein ATPase. *European Journal of Biochemistry*. 1997, 244:664-673.
43. Palmeira, A. *et. al.* Three Decades of Pgp Inhibitors: Skimming Through Several Generations and Scaffolds. *Current Medicinal Chemistry*. 2012, 19:1946-2025.
44. Yusa, K. *et. al.* Reversal Mechanism of Multidrug Resistance by Verapamil: Direct Binding of Verapamil to P-Glycoprotein on Specific Sites and Transport of Verapamil Outward across the Plasma Membrane of K562/ADM Cells. *Cancer Research*. 1989, 49:5002-5006.
45. List, A.F. *et. al.* Benefit of Cyclosporine Modulation of Drug Resistance in Patients with Poor-Risk Acute Myeloid Leukemia: a Southwest Oncology Group Study. *Blood*. 2001, 98:3212-3220.

46. Takara, K. *et. al.* Nicardipine and Itraconazole Inhibited Transcellular Transport of Digoxin. *Pharmacy and Pharmacology Communications*. 2010, 6:167-171.
47. Lehnert, M. *et. al.* Phase II Trial of Dexverapamil and Epirubicin in Patients with Non-Responsive Metastatic Breast Cancer. *Clinical Oncology*. 1998, 77:1155-1163.
48. Kolitz, J.E. *et. al.* A Randomized Comparison of Induction Therapy for Untreated Acute Myeloid Leukemia (AML) in Patients < 60 Years using P-Glycoprotein (Pgp) Modulation with Valspodar (PSC833): Preliminary Results of Cancer and Leukemia Group B Study 19808. *Blood*. 2005, 106:407.
49. Libby, E. *et. al.* Dismounting the MDR Horse. *Blood*. 2010, 116: 4037-4038.
50. Rubin, E.H. *et. al.* A Phase I Trial of a Potent P-Glycoprotein Inhibitor, Zosuquidar.3HCl Trihydrochloride (LY335979), Administered Orally in Combination with Doxorubicin in Patients with Advanced Malignancies. *Clinical Cancer Research*. 2002, 8:3710-3717.
51. Wong, H.L. *et. al.* Simultaneous Delivery of Doxorubicin and GG918 (Elacridar) by new Polymer-Lipid Hybrid Nanoparticles (PLN) for Enhanced Treatment of Multidrug-Resistant Breast Cancer. *Journal of Controlled Release*. 2006, 116:275-284.
52. Chi, K.N. *et. al.* A Phase I Pharmacokinetic Study of the P-glycoprotein Inhibitor, ONT-093, in combination with Paclitaxel in Patients with Advanced Cancer. *Investigational New Drugs*. 2005, 23:311-315.
53. Puzstai, L. *et. al.* Phase II Study of Tariquidar, a Selective P-glycoprotein Inhibitor, in Patients with Chemotherapy-Resistant, Advanced Breast Carcinoma. *Cancer*. 2005, 104:682-691.
54. Lee, B.D. *et. al.* Synthesis and Evaluation of Dihydropyrroloquinolines that Selectively Antagonize P-Glycoprotein. *Journal of Medicinal Chemistry*. 2004, 47:1413-1422.

55. Borowski, E. *et. al.* Strategies for Overcoming ABC-Transporters-Mediated Multidrug Resistance (MDR) of Tumor Cells. *Acta Biochemica Polonica*. 2005, 52:609-627.
56. Cory, T.C. *et. al.* Alterations in P-glycoprotein Expression and Function between Macrophage Subsets. *Pharmaceutical Research*. 2016, 33:2713-2721.
57. Perez-Ruiz, E. *et. al.* Cancer Immunotherapy Resistance based on Immune Checkpoint Inhibitors: Targets, Biomarkers, and Remedies. *Drug Resistance Updates*. 2020, 53:1-11.
58. Fojo, A.T. *et. al.* Expression of a Multidrug-Resistance Gene in Human Tumors and Tissues. *Proceedings of the National Academy of Sciences*. 1987, 84:265-269.
59. Thiebaut, F. *et. al.* Cellular Localization of the Multidrug-Resistance Gene Product P-glycoprotein in Normal Human Tissues. *Proceedings of the National Academy of Sciences*. 1987, 84:7735-7738.
60. Robey, R.W. *et. al.* ABC Transporters: Unvalidated Therapeutic Targets in Cancer and the CNS. *Anti-Cancer Agents in Medicinal Chemistry*. 2010, 10:625-633.
61. Lu, D. *et. al.* Multidrug Resistance-Associated Biomarkers PGP, GST-II, Topo-II and LRP as Prognostic Factors in Primary Ovarian Carcinoma. *British Journal of Biomedical Science*. 2016, 68:69-74.
62. To, K.K.W. MicroRNA: a Prognostic Biomarker and a Possible Druggable Target for Circumventing Multidrug Resistance in Cancer Chemotherapy. *Journal of Biomedical Science*. 2013, 20:99.
63. de Souza, P.S. *et. al.* Membrane Microparticles: Shedding New Light into Cancer Cell Communication. *Cancer Research*. 2016, 142:1395-1406.
64. Gonzalez, H. *et. al.* Roles of the Immune System in Cancer: from Tumor Initiation to Metastatic Progression. *Genes & Development*. 2018, 32:1267-1284.

65. Miremadi, A. *et. al.* Cancer Genetics of Epigenetic Genes. *Human Molecular Genetics*. 2007, 16:28-49.
66. Wajapeyee, N. *et. al.* Epigenetic Alterations and Mechanisms that Drive Resistance to Targeted Cancer Therapies. *Cancer Research*. 2021, 81:5589-5595.
67. Wang, N. *et. al.* Targeting Epigenetic Regulators to Overcome Drug Resistance in Cancers. *Signal Transduction and Targeted Therapy*. 2023, 8:1-24.
68. Rossi, C. *et. al.* Breast Cancer in the Era of Integrating “Omics” Approaches. *Oncogenesis*. 2022, 11:17.
69. Vasaikar, S.V. *et. al.* LinkedOmics: Analyzing Multi-Omics Data within and across 32 Cancer Types. *Nucleic Acids Research*. 2018, 46:956-963.
70. Berman, H.M. *et. al.* The Protein Data Bank. *Nucleic Acids Research*. 2000, 28:235-242.
71. Nosol, K. *et. al.* Cryo-EM Structures Reveal Distinct Mechanisms of Inhibition of the Human Multidrug Transporter ABCB1. *Proceedings of the National Academy of Sciences*. 2020, 117:26245-26253.
72. Jackson, S.M. *et. al.* Structural Basis of Small-Molecule Inhibition of Human Multidrug Transporter ABCG2. *Nature Structural & Molecular Biology*. 2018, 25:333-340.
73. Jumper, J. *et. al.* Highly Accurate Protein Structure Prediction with AlphaFold. *Nature*. 2021, 596:583-589.
74. Wishart, D.S. *et. al.* DrugBank: A Comprehensive Resource for *In Silico* Drug Discovery and Exploration. *Nucleic Acids Research*. 2006, 34:668-672.
75. Benson, D.A. *et. al.* GenBank. *Nucleic Acids Research*. 2013, 41:36-42.
76. The UniProt Consortium. UniProt: the Universal Protein Knowledgebase in 2023. *Nucleic Acids Research*. 2023, 51:523-531.

77. Gaulton, A. *et al.* ChEMBL: a Large-Scale Bioactivity Database for Drug Discovery. *Nucleic Acids Research*. 2011, 40:1100-1107.
78. Kanehisa, M. *et al.* Data, Information, Knowledge and Principle: Back to Metabolism in KEGG. *Nucleic Acids Research*. 2014, 42:199-205.
79. Wang, Y. *et al.* PubChem: A Public Information System for Analyzing Bioactivities of Small Molecules. *Nucleic Acids Research*. 2009, 37:623-633.
80. Wishart, D.S. *et al.* Using DrugBank for *In Silico* Drug Exploration and Discovery. *Current Protocols in Bioinformatics*. 2016, 54:14.4.1-14.4.31.
81. Kawas, E. *et al.* BioMoby Extensions to the Taverna Workflow Management and Enactment Software. *BMC Bioinformatics*. 2006, 7:523.
82. Rebhan, M. *et al.* GeneCards: a Novel Functional Genomics Compendium with Automated Data Mining and Query Reformulation Support. *Bioinformatics*. 1998, 14:656-664.
83. Kitson, D.H. *et al.* Functional Annotation of Proteomic Sequences based on Consensus of Sequence and Structural Analysis. *Briefings in Bioinformatics*. 2002, 3:32-44.
84. Wishart, D.S. *et al.* DrugBank: A Knowledgebase for Drugs, Drug Actions and Drug Targets. *Nucleic Acids Research*. 2008, 36:901-906.
85. Knox, C. *et al.* DrugBank 3.0: A Comprehensive Resource for ‘Omics’ Research on Drugs. *Nucleic Acids Research*. 2011, 39:1035-1041.
86. Law, V. *et al.* DrugBank 4.0: Shedding New Light on Drug Metabolism. *Nucleic Acids Research*. 2014, 42:1091-1097.
87. Wishart, D.S. *et al.* DrugBank 5.0: A Major Update to the DrugBank Database for 2018. *Nucleic Acids Research*. 2018, 46:1074-1082.

88. Knox, C. *et. al.* DrugBank 6.0: The DrugBank Knowledgebase for 2024. *Nucleic Acids Research*. 2024, 52:1265-1275.
89. Basu, A. *et. al.* An Interactive Resource to Identify Cancer Genetic and Lineage Dependencies Targeted by Small Molecules. *Cell*. 2013, 154:1151-1161.
90. Yang, W. *et. al.* Genomics of Drug Sensitivity in Cancer (GDSC): A Resource for Therapeutic Biomarker Discovery in Cancer Cells. *Nucleic Acids Research*. 2013, 41:955-961.
91. Corsello, S.M. *et. al.* Discovering the Anti-Cancer Potential of Non-Oncology Drugs by Systematic Viability Profiling. *Nature Cancer*. 2020, 1:235-248.
92. Ghandi, M. *et. al.* Next-Generation Characterization of the Cancer Cell Line Encyclopedia. *Nature*. 2019, 569:503-508.
93. Barretina, J. *et. al.* The Cancer Cell Line Encyclopedia Enables Predictive Modeling of Anticancer Drug Sensitivity. *Nature*. 2012, 483:603-607.
94. Tsherniak, A. *et. al.* Defining a Cancer Dependency Map. *Cell*. 2017, 170:564-576.
95. The Cancer Genome Atlas Research Network *et. al.* The Cancer Genome Atlas Pan-Cancer Analysis Project. *Nature Genetics*. 2013, 45:1113-1120.
96. Ehrlich, P. *et. al.* The Collected Papers of Paul Ehrlich in Four Volumes Including a Complete Bibliography. Vol. II Immunology and Cancer Research (English translation). (Pergamon, 1957).
97. Bosch, F. *et. al.* The Contributions of Paul Ehrlich to Pharmacology: A Tribute on the Occasion of the Centenary of His Nobel Prize. *Pharmacology*. 2008, 82:171-179.
98. Hill, A.V. The Possible Effects of the Aggregation of the Molecules of Haemoglobin on its Dissociation Curves. *Proceedings of the Physiological Society*, 4 (1910).

99. Gesztelyi, R. *et. al.* The Hill Equation and the Origin of Quantitative Pharmacology. *Archive for History of. Exact Sciences.* 2012, 66:427-438.
100. Omura, T. *et. al.* A New Cytochrome in Liver Microsomes. *Journal of Biological Chemistry.* 1962, 237:1375-1376.
101. Wrighton, S.A. *et. al.* The Human Hepatic Cytochromes P450 Involved in Drug Metabolism. *Critical Reviews in Toxicology.* 1992, 22:1-21.
102. McDonnell, A.M. *et. al.* Basic Review of the Cytochrome P450 System. *Journal of the Advanced Practitioner in Oncology.* 2013, 4:263-268.
103. Meijerman, I. *et. al.* Combined Action and Regulation of Phase II Enzymes and Multidrug Resistance Proteins in Multidrug Resistance in Cancer. *Cancer Treatment Reviews.* 2008, 34:505-520.
104. Runge, D. *et. al.* Induction of Cytochrome P450 (CYP) 1A1, CYP1A2, and CYP3A4 but not of CYP2C9, CYP2C19, Multidrug Resistance (MDR-1) and Multidrug Resistance Associated Protein (MRP-1) by Prototypical Inducers in Human Hepatocytes. *Biochemical and Biophysical Research Communications.* 2000, 273:333-341.
105. Benet, L.Z. *et. al.* Intestinal MDR Transport Proteins and P-450 Enzymes as Barriers to Oral Drug Delivery. *Journal of Controlled Release.* 1999, 62:25-31.
106. Faber, K.N. *et. al.* Drug Transport Proteins in the Liver. *Advanced Drug Delivery Reviews.* 2003, 55:107-124.
107. Oostendorp, R.L. *et. al.* The Biological and Clinical Role of Drug Transporters at the Intestinal Barrier. *Cancer Treatment Reviews.* 2009, 35:137-147.
108. Inui, K.I. *et. al.* Cellular and Molecular Aspects of Drug Transport in the Kidney. *Kidney International.* 2000, 58:944-958.

109. Su, L. *et. al.* Drug Transporter, P-glycoprotein (MDR1), is an Integrated Component of the Mammalian Blood-Testis Barrier. *The International Journal of Biochemistry & Cell Biology*. 2009, 41:2578-2587.
110. Ebinger, M. *et. al.* ABC Drug Transporter at the Blood-Brain Barrier. *European Archives of Psychiatry and Clinical Neuroscience*. 2006, 256:294-298.
111. Szakacs, G. *et. al.* Targeting Multidrug Resistance in Cancer. *Nature Reviews Drug Discovery*. 2006, 5:219-234.
112. Ploeger, B.A. *et. al.* Incorporating Receptor Theory in Mechanism-Based Pharmacokinetic-Pharmacodynamic (PK-PD) Modeling. *Drug Metabolism and Pharmacokinetics*. 2009, 24:3-15.
113. Southwood, Robin, Virginia H. Fleming and Gary Huckaby. *Concepts in Clinical Pharmacokinetics*. 7th ed., American Society of Health-System Pharmacists, 2018.
114. Raviv, Y. *et. al.* Photosensitized Labeling of a Functional Multidrug Transporter in Living Drug-Resistant Tumor Cells. *Journal of Biological Chemistry*. 1990, 265:3975-3980.
115. Michaelis, L. *et. al.* Die Kinetik der Invertinwirkung. *Biochemische Zeitschrift*. 1913, 49:333-369.
116. Johnson, K.A. *et. al.* The Original Michaelis Constant: Translation of the 1913 Michaelis-Menten Paper. *Biochemistry*. 2011, 50:8264-8269.
117. Nikaido, H. Prevention of Drug Access to Bacterial Targets: Permeability Barriers and Active Efflux. *Science*. 1994, 264:382-388.
118. Mitchell, P. A General Theory of Membrane Transport from Studies of Bacteria. *Nature*. 1957, 180:134-136.

119. Seelig, A. The Role of Size and Charge for Blood-Brain Barrier Permeation of Drugs and Fatty Acids. *Journal of Molecular Neuroscience*. 2007, 33:32-41.
120. Schomburg, I. *et. al.* BRENDA, Enzyme Data and Metabolic Information. *Nucleic Acids Research*. 2002, 30:47-49.
121. Chang, A. *et. al.* BRENDA, the ELIXIR Core Data Resource in 2021: New Developments and Updates. *Nucleic Acids Research*. 2021, 49:498-508.
122. Tolson, A.H. *et. al.* Regulation of Drug-Metabolizing Enzymes by Xenobiotic Receptors: PXR and CAR. *Advanced Drug Delivery Reviews*. 2011, 62:1238-1249.
123. Xu, C. *et. al.* Induction of Phase I, II and III Drug Metabolism/Transport by Xenobiotics. *Archives of Pharmacol Research*. 2005, 28:249-268.
124. Harmsen, S. *et. al.* PXR-Mediated Induction of P-glycoprotein by Anticancer Drugs in a Human Colon Adenocarcinoma-Derived Cell Line. *Cancer Chemotherapy and Pharmacology*. 2010, 66:765-771.
125. Oladimeji, P.O. *et. al.* PXR: More than just a Master Xenobiotic Receptor. *Molecular Pharmacology*. 2018, 93:119-127.
126. Lee, T.D. *et. al.* A High-Throughput Screen of a Library of Therapeutics Identifies Cytotoxic Substrates of P-glycoprotein. *Molecular Pharmacology*. 2019, 96:629-640.
127. Roovers, D.J. *et. al.* Idarubicin Overcomes P-glycoprotein-Related Multidrug Resistance: Comparison with Doxorubicin and Daunorubicin in Human Multiple Myeloma Cell Lines. *Leukemia Research*. 1999, 23:539-548.
128. Smeets, M.E.P. *et. al.* Idarubicin DNA Intercalation is Reduced by MRP1 and not Pgp. *Leukemia*. 1999, 13:1390-1398.

129. Eneroth, A. *et. al.* Evaluation of a Vincristine Resistant Caco-2 Cell Line for Use in a Calcein AM Extrusion Screening Assay for P-glycoprotein Interaction. *European Journal of Pharmaceutical Sciences*. 2001, 12:205-214.

APPENDIX A: PROTOCOLS

Protocol 1: Calcein AM Inhibitor Screen with DU4475 Cells

Materials to Prepare:

1. 500 ml Phosphate Buffered Saline (PBS): sterile filter 500 ml PBS
2. ~1 ml 47 μ M Calcein AM in dimethyl sulfoxide (DMSO)/PBS
 - a. Take up 50 μ g/vial in 50 μ l DMSO for a 1 mM stock
 - b. Add 1 ml PBS to be sure to take up all Calcein AM
3. T75 flasks of 13 ml cells/media for cells
4. Plasticware: 1 96 well black plate, multi-inhibitor reference plate, 3 15 ml conical tubes (Stain/Cells/Calcein AM), 2 50 ml conical tubes (Cells/Waste), 2 pipette basins, 2 Eppendorf tubes (count Cells)

Buffer Exchange Cells: remove FBS esterase enzymes and phenol-red

5. Remove 13 ml cells/media from 4 T75 flasks of cells
6. Centrifuge cells/media at 130 RCF for 7 min
7. Resuspend cells in 10 ml trypsin
8. Leave cells in 37 °C incubator for ~5 min
9. Add 10 ml media to cells/trypsin
10. Centrifuge 20 ml cells/trypsin at 130 RCF for 7 min
11. Resuspend cells in 20 ml sterile PBS
12. Take sample of cells of counting
13. Count cells with hemocytometer and trypan blue

14. Add sterile PBS to cells for 100,000 cells/well and pour into pipette basin

a. μl of Cells

$$100,000 \text{ cells/well} \times 12,000 \text{ Total } \mu\text{l of Needed} / (\text{_____ cells/ml} \times 0.1) =$$

μl of Cells

b. μl of PBS

$$\text{_____ Total } \mu\text{l Needed} - \text{_____ } \mu\text{l of Cells} = \text{_____ } \mu\text{l of PBS Needed}$$

15. Plate 100 μl of cells/PBS to ALL wells of 96 well plate (moving left to right)

Make Pgp Inhibitor Solutions: already in multi-inhibitor reference plate

16. Add 100 μl of multi-inhibitor reference plate wells to wells of 96 well plate (same layout, moving left to right)

17. Add 100 μl of 1% DMSO in PBS solution to wells A11 to H12 of 96 well plate

Make Staining Solution: conduct during centrifugation above

18. Make 12 ml staining solution:

a. 11,910 μl sterile PBS

b. 90 μl 47 μM Calcein AM stock (0.36 μM , 0.12 μM in 1:1:1 with Calcein AM, inhibitor and cells)

19. Pour staining solution into pipette basin

20. Add 100 μl of Stain to 100 μl cells/PBS (all wells of 96 well plate, moving left to right)

Stain Cells:

21. Measure fluorescence using plate reader (Fluorescence kinetic assay, measure every 10 minutes for 6 hours at 5% CO_2 and 37 $^\circ\text{C}$ with lid on)

22. Save the data on OneDrive

23. Export the data to Excel

Protocol 2: Calcein AM Drug Screen with DU4475 Cells

Materials to Prepare:

1. 500 ml Phosphate Buffered Saline (PBS): sterile filter 500 ml PBS
2. ~1 ml 47 μ M Calcein AM in dimethyl sulfoxide (DMSO)/PBS
 - a. Take up 50 μ g/vial in 50 μ l DMSO for a 1 mM stock
 - b. Add 1 ml PBS to be sure to take up all Calcein
3. 4 T75 flasks of 13 ml cells/media
4. Plasticware: multi-experiment reference plate, 1 96 well black plate, 3 15 ml conical tubes (Stain/Cells/Calcein AM), 2 50 ml conical tubes (Cells/Waste), 3 pipette basins, 2 Eppendorf tubes (count Cells)

Buffer Exchange Cells: remove FBS esterase enzymes and phenol-red

5. Remove 13 ml cells/media from 4 T75 flasks of cells
6. Centrifuge cells/media at 130 RCF for 7 min
7. Resuspend cells in 10 ml trypsin
8. Leave cells in 37 °C incubator for ~5 min
9. Add 10 ml media to cells/trypsin
10. Centrifuge 20 ml cells/trypsin at 130 RCF for 7 min
11. Resuspend cells in 20 ml sterile PBS
12. Take sample of cells for counting
13. Count cells with hemocytometer and trypan blue
14. Add sterile PBS to cells for 100,000 cells/well and pour into pipette basin
 - a. μ l of Cells

$$100,000 \text{ cells/well} \times 12,000 \text{ Total } \mu\text{l of Needed} / (\text{_____ cells/ml} \times 0.1) =$$

μl of Cells

b. μl of PBS

_____ Total μl Needed - _____ μl of Cells = _____ μl of PBS Needed

15. Plate 100 μl of cells/PBS to all wells of 96 well plate (moving right to left)

Make Pgp Inhibitor Solutions: already in multi-experiment plate

16. Pour sterile PBS into pipette basin

17. Add 70 μl sterile PBS to all wells of 96 well plate (moving right to left)

18. Add 30 μl of multi-experiment plate wells to all wells of 96 well plate (same layout, moving right to left)

Make Staining Solution: conduct during centrifugation above

19. Make 12 ml staining solution:

a. 11,910 μl sterile PBS

b. 90 μl 47 μM new Calcein AM stock (0.36 μM, 0.12 μM in 1:1:1 with Calcein AM, drug and cells)

20. Pour staining solution into pipette basin

21. Add 100 μl of Stain to all wells of 96 well plate (moving right to left)

Stain Cells:

22. Measure fluorescence using plate reader (Fluorescence kinetic assay, measure every 10 minutes for 6 hours at 5% CO₂ and 37 °C with lid on)

23. Save the data on OneDrive

24. Export the data to Excel

Protocol 3: Pgp Quantification using Flow Cytometry

Make Solutions:

“MACS” Buffer (filter) = Ab-Ice-Stain

- 500 ml pH 7.4 Phosphate Buffered Saline (PBS)
- 0.5 mM Ethylenediaminetetraacetic acid (EDTA) (1:1000 dilution) (molecular grade)
- 1% Bovine Serum Albumin (BSA) (1 g/100 ml)

PBS Buffer (filter) = FACS

- 500 ml pH 7.4 PBS

Buffer Exchange/Concentrate Cells:

1. Buffer exchange 1 T75 flask for each cell line to approximately 1 million/ml density
 - a. NOTE 1: 1 confluent T75 flask = 20 million cells
 - i. 1 confluent 9 cm petridish = 10 million cells
 - b. NOTE 2: trypsinize adherent cell lines (Caco-2, DU4475)
2. Spin down cells in conical tube (130 g 7 min)
3. Wash cells 1x 10-15 ml in MACS Buffer
4. Take up each pellet in MACS Buffer with pre-determined volume

Antibody Staining:

5. Add 4x 100 μ l aliquots into Eppendorf tubes
6. Add 4 μ l of Block for 3 μ M IgG and incubate for 5 min at room temperature
 - a. NOTE: 4 μ l x 6 lines x 4 replicates = 96 μ l total
7. Add 2x 10 μ l (10x dilution) of Isotype Control to Control Rows
8. Add 2x 10 μ l (10x dilution) of anti-Pgp to Pgp-Stain rows
 - a. NOTE: 10 μ l x 6 lines x 2 replicates = 0.120 ml total

i. STOCK: $0.1 \text{ mg}/200 \text{ } \mu\text{l} = 0.5 \text{ mg}/\text{ml} = 333 \text{ nM}$

9. Incubate on ice for 30 min

Flow Cytometry Preparation:

10. Set centrifuge temperature to 4 °C and 130 RCF

11. Add 1 ml MACS Buffer, spin down and pour out (5 min 130 RCF)

12. Add 1 ml MACS Buffer, spin down and pour out (5 min 130 RCF)

13. Add 100 μl PBS + put on ice (5 min 130 RCF)

Flow Cytometry on Antibody-Stained Cells:

14. Check SIP to make sure it has DI water on it

15. Check Fluid Tank levels:

a. Sheath (blue), bleach (yellow) and detergent (green)

16. Check Waste Tank (red) level

17. Turn on Instrument (takes ~15 minutes to start up)

18. Check settings of instrument:

a. Run limited to 10,000 events

b. Speed: medium

19. Run DI water for ~ 2 minutes until the # of events is ~0-2

20. Run Unlabeled sample (no antibody) to establish FSC/SSC gating

21. Make a new histogram plot that is gated on the interior of the FSC/SSC gate

22. Change the histogram x-axis to your fluorophore of interest (Phycoerythrin-Ab) by

clicking on the x-axis labeled

23. Proceed to take all samples

Beads Calibration Procedure:

24. SET UP BLANK

- a. Add one drop of the reference blank “B” to 400 μ l suspending solution (PBS)
- b. Analyze the microspheres on the flow cytometer
- c. Adjust flow rate to 100 beads/second is recommended
- d. Gate FSC vs SSC around the singlet population of the microspheres
- e. Create a fluorescence histogram for phycoerythrin, including only gate above
- f. Verify that the reference blank population appears near the origin of the histogram

25. SETUP CALIBRATION PLOT

- a. Combine 1 drop of each bottle (not blank) to 400 μ l of the same type of buffer for analysis
- b. Analyze the microspheres on the flow cytometer
- c. Discernable fluorescence peaks should be observed

Flow Cytometry Cleanup:

26. Run SIP clean
27. Turn off instrument

Protocol 4: Plate-based Assay with Pgp Inhibitor

Materials to Prepare:

1. 500 ml Phosphate Buffered Saline (PBS): Sterile filter 500 ml PBS
2. ~1 ml 80 μ M Calcein AM in dimethyl sulfoxide (DMSO)/PBS:
 - a. Take up 50 μ g/vial in 50 μ l DMSO for a 1 mM stock
 - b. Add 1 ml PBS to be sure to take up all Calcein
3. 2 T75 flasks of 13 ml cells/media
4. Plasticware: 96 well black plate, 24 well clear plate, 3 15 ml conical tubes (Stain/Cells), 50 ml conical tube (Cells), 2 pipette basins, 2 Eppendorf tubes (count Cells)

Buffer Exchanged Cells: remove FBS esterase enzymes and phenol-red

5. Remove 13 ml cells/media from 2 T75 flasks
6. Centrifuge cells/media at 130 RCF for 7 min
7. Resuspend cells in 6 ml trypsin
8. Leave cells in 37 °C incubator for 3 min
9. Add 6 ml media to cells/trypsin
10. Centrifuge 12 ml cells/trypsin at 130 RCF for 7 min
11. Resuspend cells in 6 ml sterile PBS
12. Take sample of cells for counting
13. Count cells with hemocytometer and trypan blue
14. Add sterile PBS to cells for 100,000 cells/well and pour into pipette basin

μ l of Cells

100,000 cells/well x 7,000 Total μ l of Needed / (_____ cells/ml x 0.1) = _____ μ l

of Cells

μl of PBS

_____ Total μl Needed - _____ μl of Cells = _____ μl of PBS Needed

15. Plate 100 μl of cells/PBS to wells A1-C1, F1-H1 to A9-C9, F9-H9 of 96 well plate

16. Add 100 μl of PBS only to wells A9-C9, F9-H9 of 96 well plate

Make Oncology Drug Solutions: serial dilutions

17. Make Paclitaxel and Zosuquidar serial dilutions in 24 well clear plate

a. Paclitaxel 5X dilutions

- i. $10,000,000 \text{ nM} * 30 \text{ } \mu\text{l} = 150,000 \text{ nM} * 2,000 \text{ } \mu\text{l}$ (well A1)
- ii. $150,000 \text{ nM} * 400 \text{ } \mu\text{l} = 30,000 \text{ nM} * 2,000 \text{ } \mu\text{l}$ (well A2)
- iii. $30,000 \text{ nM} * 400 \text{ } \mu\text{l} = 6,000 \text{ nM} * 2,000 \text{ } \mu\text{l}$ (well A3)
- iv. $6,000 \text{ nM} * 400 \text{ } \mu\text{l} = 1,200 \text{ nM} * 2,000 \text{ } \mu\text{l}$ (well A4)
- v. $1,200 \text{ nM} * 400 \text{ } \mu\text{l} = 240 \text{ nM} * 2,000 \text{ } \mu\text{l}$ (well A5)
- vi. $240 \text{ nM} * 400 \text{ } \mu\text{l} = 48 \text{ nM} * 2,000 \text{ } \mu\text{l}$ (well A6)
- vii. $48 \text{ nM} * 400 \text{ } \mu\text{l} = 9.6 \text{ nM} * 2,000 \text{ } \mu\text{l}$ (well B1)
- viii. $9.6 \text{ nM} * 400 \text{ } \mu\text{l} = 1.92 \text{ nM} * 2,000 \text{ } \mu\text{l}$ (well B2)
- ix. Control 1,000 μl PBS (well B3)

b. Zosuquidar 10X dilutions

- i. $10,000,000 \text{ nM} * 3 \text{ } \mu\text{l} = 150,000 \text{ nM} * 2,000 \text{ } \mu\text{l}$ (well C1)
- ii. $15,000 \text{ nM} * 200 \text{ } \mu\text{l} = 1,500 \text{ nM} * 2,000 \text{ } \mu\text{l}$ (well C2)
- iii. $1,500 \text{ nM} * 200 \text{ } \mu\text{l} = 150 \text{ nM} * 2,000 \text{ } \mu\text{l}$ (well C3)
- iv. $150 \text{ nM} * 200 \text{ } \mu\text{l} = 15 \text{ nM} * 2,000 \text{ } \mu\text{l}$ (well C4)
- v. $15 \text{ nM} * 200 \text{ } \mu\text{l} = 1.5 \text{ nM} * 2,000 \text{ } \mu\text{l}$ (well C5)
- vi. $1.5 \text{ nM} * 200 \text{ } \mu\text{l} = 0.15 \text{ nM} * 2,000 \text{ } \mu\text{l}$ (well C6)

- vii. $0.15 \text{ nM} * 200 \mu\text{l} = 0.015 \text{ nM} * 2,000 \mu\text{l}$ (well D1)
- viii. $0.015 \text{ nM} * 200 \mu\text{l} = 0.0015 \text{ nM} * 2,000 \mu\text{l}$ (well D2)
- ix. Control 1,000 μl PBS (well D3)

18. Add 100 μl of Paclitaxel and Zosuquidar serial dilutions to 100 μl cells/PBS (wells A1-C1, F1-H1 to A8-C8, F8-H8 96 well plate), in 1:1:1 with cells in stain:

a. Paclitaxel 5X dilutions

- i. $150,000 \text{ nM} * 100 \mu\text{l} = 50,000 \text{ nM} * 300 \mu\text{l}$ (A1-C1)
- ii. $30,000 \text{ nM} * 100 \mu\text{l} = 10,000 \text{ nM} * 300 \mu\text{l}$ (A2-C2)
- iii. $6,000 \text{ nM} * 100 \mu\text{l} = 2,000 \text{ nM} * 300 \mu\text{l}$ (A3-C3)
- iv. $1,200 \text{ nM} * 100 \mu\text{l} = 400 \text{ nM} * 300 \mu\text{l}$ (A4-C4)
- v. $240 \text{ nM} * 100 \mu\text{l} = 80 \text{ nM} * 300 \mu\text{l}$ (A5-C5)
- vi. $48 \text{ nM} * 100 \mu\text{l} = 16 \text{ nM} * 300 \mu\text{l}$ (A6-C6)
- vii. $9.6 \text{ nM} * 100 \mu\text{l} = 3.2 \text{ nM} * 300 \mu\text{l}$ (A7-C7)
- viii. $1.92 \text{ nM} * 100 \mu\text{l} = 0.64 \text{ nM} * 300 \mu\text{l}$ (A8-C8)
- ix. 0 nM (A9-C9)

b. Zosuquidar 10X dilutions

- i. $15,000 \text{ nM} * 100 \mu\text{l} = 5,000 \text{ nM} * 300 \mu\text{l}$ (F1-H1)
- ii. $1,500 \text{ nM} * 100 \mu\text{l} = 500 \text{ nM} * 300 \mu\text{l}$ (F2-H2)
- iii. $150 \text{ nM} * 100 \mu\text{l} = 50 \text{ nM} * 300 \mu\text{l}$ (F3-H3)
- iv. $15 \text{ nM} * 100 \mu\text{l} = 5 \text{ nM} * 300 \mu\text{l}$ (F4-H4)
- v. $1.5 \text{ nM} * 100 \mu\text{l} = 0.5 \text{ nM} * 300 \mu\text{l}$ (F5-H5)
- vi. $0.15 \text{ nM} * 100 \mu\text{l} = 0.05 \text{ nM} * 300 \mu\text{l}$ (F6-H6)
- vii. $0.015 \text{ nM} * 100 \mu\text{l} = 0.005 \text{ nM} * 300 \mu\text{l}$ (F7-H7)

viii. $0.0015 \text{ nM} * 100 \mu\text{l} = 0.0005 \text{ nM} * 300 \mu\text{l}$ (F8-H8)

ix. 0 nM (F9-H9)

Make Staining Solution: conduct during centrifugation above

19. Make 10 ml staining solution:

a. 9,925 μl sterile PBS

b. 75 μl 80 μM Calcein AM stock (0.6 μM , 0.2 μM in 1:1:1 with Calcein AM, oncology drug or PBS and cells)

20. Pour staining solution into pipette basin

21. Add 100 μl of Stain to 100 μl cells/PBS (wells A1-C1, F1-H1 through A9-C9, F9-H9 of 96 well plate)

Stain Cells:

22. Measure fluorescence using plate reader (Fluorescence kinetic assay, measure every 10 minutes for 3 hours at 5% CO₂ and 37 °C with lid on)

23. Save the data on OneDrive

24. Export the data to Excel

Protocol 5: Calcein AM with or without Pgp Inhibitor

Materials to Prepare:

1. 500 ml Phosphate Buffered Saline (PBS): sterile filter 500 ml PBS
2. ~1 ml 80 μ M Calcein in dimethyl sulfoxide (DMSO)/PBS
 - a. Take up 50 μ g/vial in 50 μ l DMSO for a 1 mM stock
 - b. Add 1 ml PBS to be sure to take up all Calcein
3. 1.5 ml Propidium iodide (PI) in water
4. 2 T75 flasks of 13 ml cells/media incubated ~24 hours with 5 μ M Zosuquidar or 0.05% DMSO
5. Plasticware: 24 well plate, 3 15 ml conical tubes

Buffer Exchange Cells: remove FBS esterase enzymes and phenol-red

6. Transfer 2 T75 flasks of DU4475 cells to 15 ml conical tubes
 - a. ~13 ml cells/media
7. Centrifuge cells at 130 RCF for 7 min
8. MAKE STAIN SOLUTION (see below)
9. Wash 1x with 13 ml sterile PBS
10. Take up cells in 13 ml sterile PBS
11. Plate 0.5 ml of cells/PBS to wells C1-C6, D1-D6 of 24 well plate

Make Staining Titration: conduct during centrifugation above

12. Make 10 ml staining solution
 - a. 10 ml sterile PBS
 - b. 0.4 ml 80 μ M Calcein stock (25x dilution for 3.2 μ M)
 - i. 134 μ l 1.5 mM PI stock (75x dilution for 20 μ M)

- ii. $5 \mu\text{M}$ Zosuquidar ($10 \text{ mM} * V = 10.534 \text{ ml} * 5 \mu\text{M}$), $V = 5.27 \mu\text{l}$ (only for + inhibitor)

13. Add 2 ml staining solution to wells A6, B6 of 24 well plate

14. Add 1.5 ml PBS to wells A1-A5, B1-B5 of 24 well plate

15. Serially dilute staining solution 4x (0.5 ml stain + 1.5 ml PBS) across A1-A5, B1-B5 of 24 well plate

Stain Cells:

16. Add 0.5 ml of Serial Diluted Stain (wells A1-A6, B1-B6) to 0.5 ml cells (wells C1-C6, D1-D6) and mix

17. Image GFP, TxRed on EVOS M5000 fluorescent microscope

18. Incubate at $37 \text{ }^\circ\text{C}$ (incubator) for 30 min

Visualize:

19. EVOS M5000 fluorescent microscope

- a. Remove 24 well plate and place on EVOS stage
- b. Adjust 2 lamp intensities to optimal for largest concentration of stain (C6, D6)
- c. Image GFP, TxRed for wells C1-C6, D1-D6
 - i. NOTE: increase lamp intensity when cells disappear

Protocol 6: Pgp Inhibitor Optimization with Calcein AM

Materials to Prepare:

1. 500 ml Phosphate Buffered Saline (PBS): sterile filter 500 ml PBS
2. ~1 ml 80 μ M Calcein in dimethyl sulfoxide (DMSO)/PBS:
 - a. Take up 50 μ g/vial in 50 μ l DMSO for a 1 mM stock
 - b. Add 1 ml PBS to be sure to take up all Calcein
3. 1.5 mM propidium iodide (PI) in water
4. 1 T75 flask of 13 ml cells/media
5. Plasticware: 48 flat well clear plate, 3 15 ml conical tubes, 7 Eppendorf tubes, pipette basin

Buffer Exchange Cells: remove FBS esterase enzymes and phenol-red

6. Transfer 1 T75 flask of DU4475 cells to 15 ml conical tube
 - a. ~13 ml cells/media
7. Centrifuge cells at 130 RCF for 7 min
8. MAKE STAIN SOLUTION (see below)
9. Wash 1x with 13 ml sterile PBS
10. Take up cells in 13 ml sterile PBS, pour into pipette basin
11. Plate 300 μ l of cells/PBS to wells C2-C7 of 48 well plate

Make Staining Titration: conduct during centrifugation above

12. Make 5 ml staining solution
 - a. 5 ml sterile PBS
 - b. 18.75 μ l 80 μ M Calcein stock (~267x dilution for 0.3 μ M)
 - c. 6.25 μ l 1.5 mM PI stock (800x dilution for 1.875 μ M)

13. Add 500 μ l staining solution to wells A2-A7 of 48 well plate

Zosuquidar Serial Dilutions:

14. Make DMSO PBS (dPBS) with 150 μ l into 15 ml PBS
15. Add 10 μ l of 10 mM stock into 990 μ l dPBS (Vial A—100 μ M)
16. Add 250 μ l of Vial A into 750 μ l dPBS (Vial B—25 μ M)
17. Add 250 μ l of Vial B into 750 μ l dPBS (Vial C—6.25 μ M)
18. Add 250 μ l of Vial C into 750 μ l dPBS (Vial D—1.56 μ M)
19. Add 250 μ l of Vial D into 750 μ l dPBS (Vial E—0.39 μ M)
20. Add 250 μ l of Vial E into 750 μ l dPBS (Vial F—0.1 μ M)
21. Add 300 μ l of Vial A into well C2
22. Add 300 μ l of Vial B into well C3
23. Add 300 μ l of Vial C into well C4
24. Add 300 μ l of Vial D into well C5
25. Add 300 μ l of Vial E into well C6
26. Add 300 μ l of Vial F into well C7

Stain Cells:

27. Add 300 μ l of Stain (wells A2-A7) to 600 μ l cells/PBS/Zosuquidar (wells C2-C7) and mix
28. Image GFP, TxRed on EVOS M5000 fluorescent microscope
29. Incubate at 37 $^{\circ}$ C (incubator) for 30 min

Visualize:

30. EVOS M5000 fluorescent microscope
 - a. Remove 48 well plate and place on EVOS stage

- b. Adjust 3 lamp intensities to optimal for largest concentration of Zosuquidar (well C2)
- c. Image GFP, TxRed for wells C2-C7
 - i. NOTE: increase lamp intensity when cells disappear